


Article

Analyses of Physical and Chemical Compositions of Different Medicinal Specifications of CRPV by Use of Multiple Instrumental Techniques Combined with Multivariate Statistical Analysis

Yang Wang ^{1,†} , Weiliang Cui ^{2,3,†}, Guowei Pang ¹, Lewen Xiong ¹, Qingzhi Liu ¹, Lili Xu ^{1,2}, Huifen Li ^{1,*} and Yongqiang Lin ^{2,*}

¹ School of Pharmacy, Shandong University of Traditional Chinese Medicine, Jinan 250355, China; wangyang961125@163.com (Y.W.); 15866682186@163.com (G.P.); lewenxiong@126.com (L.X.); qingzhi0905@163.com (Q.L.); hshpipi@163.com (L.X.)

² Shandong Institute for Food and Drug Control, Jinan 250101, China; xinyao2002@126.com

³ State Key Laboratory of Generic Manufacture Technology of Chinese Traditional Medicine, Linyi 276005, China

* Correspondence: 05000095@sducm.edu.cn (H.L.); 60030128@sducm.edu.cn (Y.L.)

† These authors contributed equally to this work.



Citation: Wang, Y.; Cui, W.; Pang, G.; Xiong, L.; Liu, Q.; Xu, L.; Li, H.; Lin, Y. Analyses of Physical and Chemical Compositions of Different Medicinal Specifications of CRPV by Use of Multiple Instrumental Techniques Combined with Multivariate Statistical Analysis. *Molecules* **2022**, *27*, 3285. <https://doi.org/10.3390/molecules27103285>

Academic Editor: Yu Yang

Received: 10 April 2022

Accepted: 17 May 2022

Published: 20 May 2022

Publisher's Note: MDPI stays neutral with regard to jurisdictional claims in published maps and institutional affiliations.



Copyright: © 2022 by the authors. Licensee MDPI, Basel, Switzerland. This article is an open access article distributed under the terms and conditions of the Creative Commons Attribution (CC BY) license (<https://creativecommons.org/licenses/by/4.0/>).

Abstract: Citri Reticulatae Pericarpium Viride (CRPV) is the processed product of *Citrus reticulata* Blanco. We systematically analyzed two CRPV types, Geqingpi (GQP) and Sihuaqingpi (SHQP), based on powder color, microscopic characteristics, and chemical composition. In addition, we characterized their constituents via ultra-high-performance liquid chromatography with hybrid quadrupole-orbitrap mass spectrometry (UHPLC-Q-Exactive Orbitrap-MS). Both showed significant differences in their powder color and microscopic characteristics. Fourier-transform infrared (FT-IR) spectroscopic analysis results showed that the C=O peak absorption of carboxylic acids and their carbonyl esters in SHQP was higher than that of GQP, while the C-OH and C-H plane bending peaks of polysaccharides were lower than those of GQP. We analyzed these data via similarity analysis, PCA, and OPLS-DA. GQP and SHQP had large distinct differences. Based on the mass measurements for molecular and characteristic fragment ions, we identified 44 main constituents from CRPV, including different flavonoid glycosides and flavonoid aglycones in SHQP and GQP, respectively. We found luteolin-6-C-glucoside, orientin, rhoifolin, and pilloin solely in SHQP, and naringenin and hesperetin only in GQP. The peak area measurements showed GQP having a higher flavonoid glycoside (narirutin, hesperidin, etc.) content, whereas SHQP had a higher polymethoxyflavone (nobiletin, tangeretin, etc.) content. Since we holistically analyzed two CRPV types, the results can not only support future pharmacological research, but also provide a scientific basis for formulating more reasonable CRPV quality standards and guide its clinical potential as a precision medicine.

Keywords: Geqingpi; Sihuaqingpi; *Citrus reticulata* Blanco; Citri Reticulatae Pericarpium Viride; flavonoid glycosides; flavonoid aglycones; polymethoxyflavones; TCM; UHPLC-Q-Exactive Orbitrap-MS; FT-IR

1. Introduction

CRPV is a traditional Chinese medicine (TCM) commonly used in China. According to the “Pharmacopoeia of the People’s Republic of China”, CRPV is the processed product of the peel of the dried young or immature fruit of *Citrus reticulata* Blanco and its cultivars. The earliest records of its medicinal application can be traced back to the Tang Dynasty in China [1]. As per the TCM theory, CRPV soothes the liver and breaks Qi, eliminates accumulation, and resolves stagnation [2]. According to its harvesting time, CRPV can be divided into two types: GQP and SHQP. GQP is the young citrus fruit and is often

collected from May to June; while SHQP, often collected from July to August, is the peel of the immature citrus fruit. When used, GQP is directly sliced, whereas SHQP is longitudinally cut into four pieces towards the base of the peel, and all the flesh pieces are removed. According to ancient Chinese herbal books, statements like “broken head-like lotus petals [3]”, “cross out the flesh and divided into four pieces called lotus-like CRPV [4]”, and “it is better to use a knife to cut the lotus petals on the CRPV”, indicate that SHQP was used in ancient China [5]. However, GQP is currently often used in the Chinese mainland. Since CRPV used in ancient and modern China has different types, the difference in composition and efficacy between the two types is worth exploring.

At present, SHQP costs twice that of GQP in the Chinese mainland. GQP, which is mainly used as the raw material of decoctions, has a market share of 80–90%. SHQP is mostly used for preparing Chinese patent medicine, and is also sold to South Korea, Hong Kong, etc. This shows that there are price and grade differences in the current commodity circulation types of CRPV. It is necessary to find the different components of the two types, to help establish the CRPV grade standards and provide a reference for the identification method of Chinese patent medicines with different CRPV.

Modern studies have found that CRPV inhibits (a) gastrointestinal smooth muscle movement [6], (b) duodenum contraction [7], (c) the movement of the longitudinal muscle strips of the small intestine, (d) the contraction of the longitudinal muscle of the ileum, and stimulating the smooth muscle of the bladder [8–10]; it also affects the bioelectrical activity of the gastrointestinal tract. It can also reduce the amplitude of the gastric electric slow-wave and prolongs the period [11].

Clinical studies have found that CRPV extract can induce apoptosis in the human colon cancer cell line SNU-C4, thus suggesting that CRPV has anticancer effects [12]. Polymethoxyflavones (PMFs) in CRPV improve metabolic disorders like hyperlipidemia, which is induced by a high-fat diet by modulating the gut microbiome and amino acid metabolism [13,14]. It also inhibits the proliferation of gastric cancer cells by inducing gastric cancer cell death via upregulation of the RAR β protein [15]. Bioactive flavonoids (narirutin, nobiletin, tangeretin, etc.) can protect the liver, reduce its damage, and prevent liver diseases [16,17]. Nobiletin may inhibit the expression of IL-6, TNF, and CCL2, which have anti-inflammatory and antioxidant properties. It can relieve the clinical symptoms of colitis mice and reduce their liver and kidney damage [18–20]. Tangeretin may inhibit the expression of interleukin-23 and other related proteins via the Notch signaling pathway, thereby treating acute lung injury [21]. At the same time, it may also inhibit the proliferation of liver cancer cells [22]. Narirutin has also exhibited anti-inflammatory and antioxidant activities, by activating the NF- κ B and MAPKs pathways, and inhibiting various pro-inflammatory mediators like NO and PGE2 in macrophages [23]. It not only has a potential therapeutic effect on Alzheimer’s disease, but may also reduce alcohol-induced liver damage [24,25]. Hesperidin has not only reduced in vivo lipid accumulation, indicating its potential anti-hyperlipidemic effects, but also has anti-osteoporotic effects [26,27].

Although some studies have shown that GQP and SHQP are mostly similar in their compositions, the contents of flavonoids (hesperidin, narirutin, nobiletin, tangeretin, etc.) and alkaloids (synephrine, N-methyltyraminehydrochloride) are significantly different. While GQP has higher narirutin and hesperidin contents than SHQP, it has comparatively lower contents of nobiletin and tangeretin [28–30]. Understanding the pharmacodynamic material basis of the two CRPV types would help in guiding their rational clinical use.

In this study, we used colorimeter, microscope, FT-IR, and UHPLC-Q-Exactive Orbitrap-MS technology to comprehensively analyze the similarities and differences between GQP and SHQP based on powder color, microscopic characteristics, and chemical composition, to provide a scientific basis for formulating more reasonable CRPV quality standards and guiding its clinical development as a precision medicine.

2. Results

2.1. Powder Color Analysis

Upon analyzing the pictures of both GQP and SHQP powder, we found the GQP powder color was darker than that of SHQP (Figure 1). Based on the L^* , a^* , and b^* values of 22 samples shown in Table 1, we can see that SHQP had a higher brightness L^* value than GQP, thereby indicating that the SHQP powder color was brighter. Although the red-green degree value a^* : $GQP > SHQP > 0$, indicated that both their powder colors were red, the SHQP color was redder. Furthermore, the yellow-blue degree value b^* : $SHQP > GQP > 0$, indicated that both their powder colors were yellow, but the color of the SHQP was yellower.

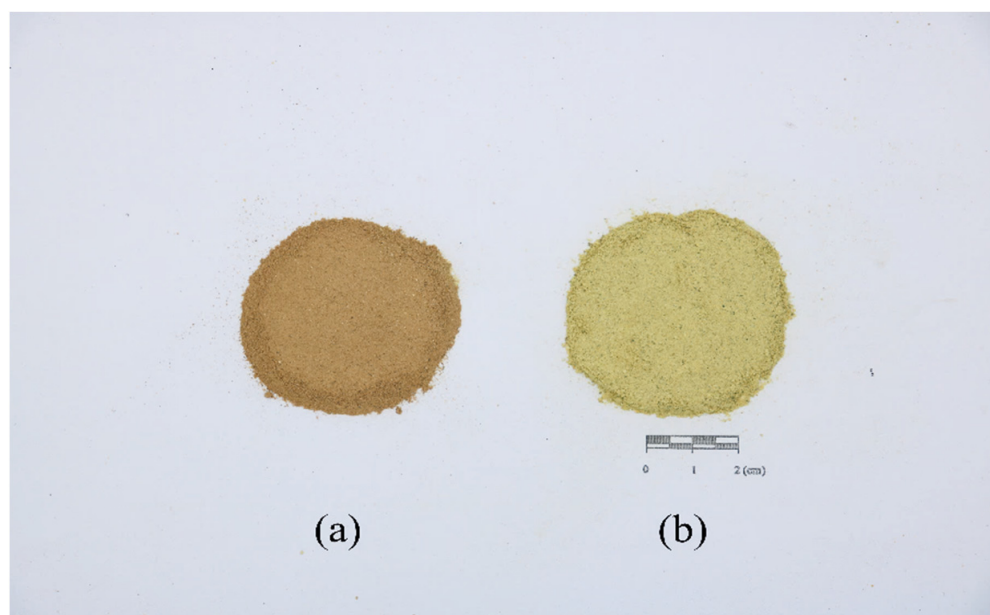


Figure 1. Powder color of CRPV: GQP (a) and SHQP (b).

Table 1. The value of L^* , a^* , and b^* of GQP and SHQP.

| Variable Name | Sample Name | |
|---------------|----------------|-------------------|
| | GQP (n = 12) | SHQP (n = 10) |
| L^* | 62.0 ± 3.9 | 72.9 ± 2.7 ▲▲ |
| a^* | 6.0 ± 0.6 | 1.6 ± 1.3 ▲▲ |
| b^* | 13.8 ± 1.7 | 19.1 ± 1.7 ▲▲ |
| E^*ab | 63.8 ± 4.1 | 75.6 ± 2.5 ▲▲ |

▲▲ $p < 0.01$, as compared with the GQP.

2.2. Microscopic Cell Analysis

According to the microscopic observation, the color of the microscopic cells of GQP was darker, while that of SHQP was lighter, thus being consistent with the powder color results. According to the Chinese Pharmacopoeia 2020 edition, while the GQP microcells comprise calcium oxalate crystallization, epidermal cells of the pulp capsule, and hesperidin crystal (a), those of SHQP mainly comprise tracheal, calcium oxalate crystallization, exocarp, mesocarp parenchyma, hesperidin crystal, and stoma (b). The result is shown in Figure 2. However, while observing, we found that the characteristic cells of SHQP also existed in individual GQP batches.

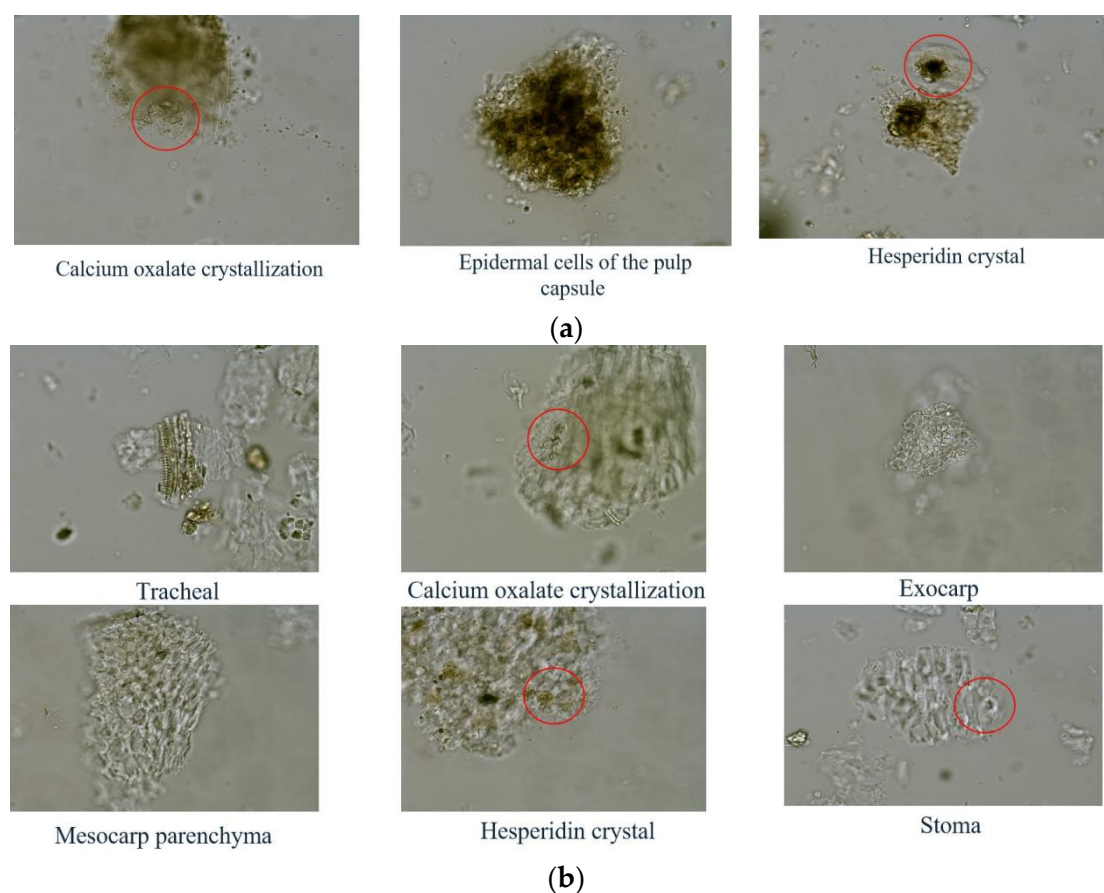


Figure 2. Cell images of the microscopic features of CRPV: GQP (a) and SHQP (b).

2.3. FT-IR Analysis

The FT-IR spectrum of CRPV is shown in Figure 3, and the location of the most relevant features of the CRPV are shown in Table 2. We divided the infrared spectral absorption peaks of GQP and SHQP into five sections: the first was $3450\text{--}3350\text{ cm}^{-1}$; the second was $3000\text{--}2800\text{ cm}^{-1}$; the third was $1800\text{--}1350\text{ cm}^{-1}$; the fourth was $1300\text{--}1000\text{ cm}^{-1}$; and the fifth section was $900\text{--}600\text{ cm}^{-1}$. There were no significant differences between GQP and SHQP in the first and second sections. Affected by volatile oils, GQP and SHQP showed characteristic peaks near 3419 cm^{-1} , which were broad and strong, resulting from the hydrogen bonding of free O-H. Due to flavonoids, GQP and SHQP showed characteristic peaks near 2923 cm^{-1} , generated by the asymmetric stretching vibration of methylene C-H. There was a significant difference between GQP and SHQP in the third sections, affected by carboxylic acids and their esters. GQP and SHQP showed characteristic peaks near 1746 cm^{-1} , which were carbonyl C=O stretching vibration peaks, with the absorption peak of SHQP in this band being more noticeable than that of GQP, leading to speculation that the content of carboxylic acids and its esters in SHQP was higher than that in GQP. GQP and SHQP showed characteristic peaks near 1639 cm^{-1} , which were C=C or aromatic ring skeleton vibration superimposed peaks. However, GQP showed two absorption peaks at 1646 cm^{-1} and 1609 cm^{-1} , due to asymmetric stretching vibrations. In the fourth and fifth sections, the absorption peaks of GQP were more noticeable than those of SHQP, with the fourth section being $1300\text{--}1000\text{ cm}^{-1}$, due mostly to C-O stretching vibration peaks, while the C-OH stretching vibration peaks of polysaccharides were mostly around 1070 cm^{-1} . The fifth segment peak of $900\text{--}600\text{ cm}^{-1}$ was mostly the vibration absorption peak of carbohydrates, affected by polysaccharides. GQP and SHQP showed characteristic peaks around 800 cm^{-1} , which were C-H plane bending vibration absorption peaks. We speculated that GQP had a higher polysaccharide content than SHQP.

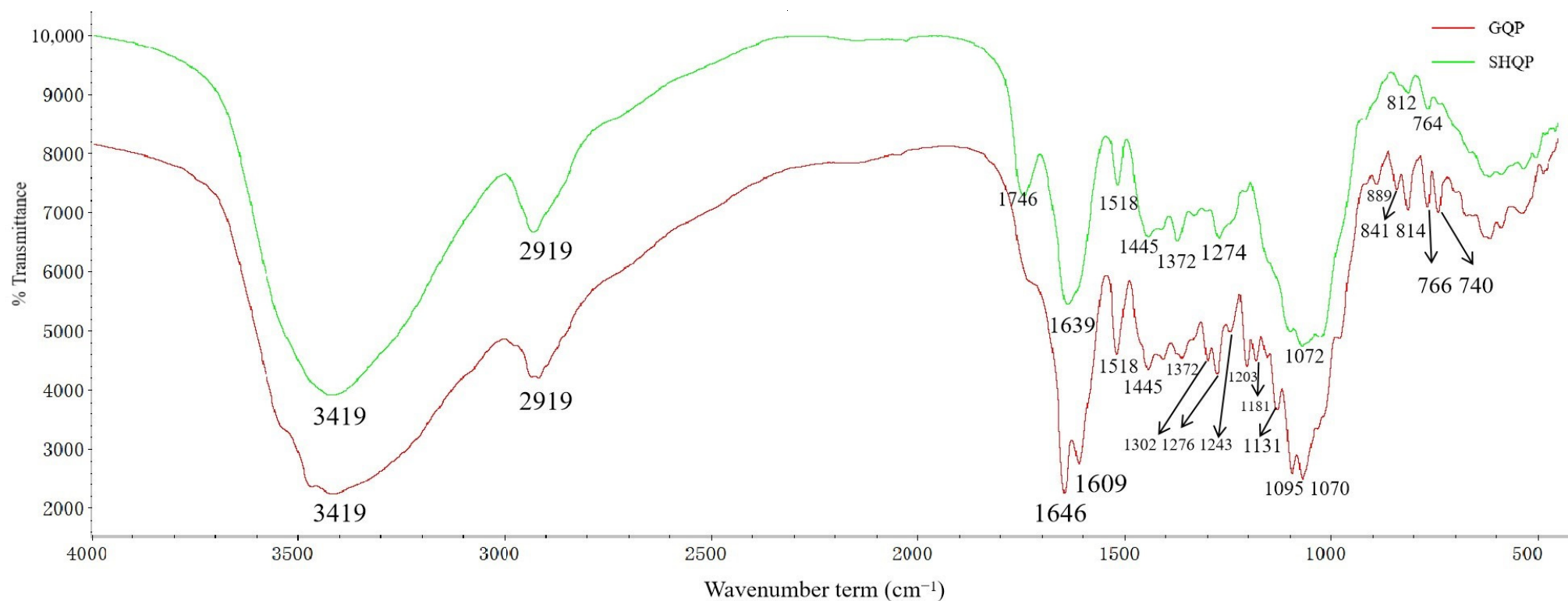


Figure 3. FT-IR of GQP and SHQP.

Table 2. Location of the most relevant features of the FT-IR spectra of the CRPV.

| Name | Wavenumber Term (cm ⁻¹) | | | | | | | | | | | | | | | | | | | | |
|------|-------------------------------------|------|------|------|------|------|------|------|------|------|------|------|------|------|------|------|-----|-----|-----|-----|-----|
| | 1 | 2 | 3 | 4 | 5 | 6 | 7 | 8 | 9 | 10 | 11 | 12 | 13 | 14 | 15 | 16 | 17 | 18 | 19 | 20 | 21 |
| GQP | 3419 | 2919 | — | 1646 | 1609 | 1518 | 1445 | 1372 | 1302 | 1276 | 1243 | 1203 | 1181 | 1131 | 1095 | 1070 | 889 | 841 | 814 | 766 | 740 |
| SHQP | 3419 | 2919 | 1746 | 1639 | — | 1518 | 1445 | 1372 | — | 1274 | — | — | — | — | — | 1072 | — | — | 812 | 764 | — |

2.4. Qualitative Analysis of Constituents

We analyzed the CRPV samples using UHPLC-Q-Exactive Orbitrap-MS in both positive and negative ion modes (Figure 4). Considering the chromatographic peaks, the MS spectra obtained in positive ion mode were better than those obtained in negative ion mode. Most of the PMFs showed abundant peaks in the positive ion mode rather than in negative ion mode. Details of the identified compounds are presented in Table 3. Finally, 44 major components were identified or preliminarily identified, including 5 flavone-C-glycosides, 4 flavone-O-glycosides, 4 flavanone-O-glycosides, 4 flavanone aglycones, 21 PMFs, 3 alkaloids, 2 limonoids, and 1 other compound (Table 3). Chemical structures of the major constituents are shown in Figures 5–7 and Tables 4 and 5. Among them, luteolin-6-C-glucoside, orientin, rhoifolin, and pilloin were unique to SHQP, most of which were flavonoid glycosides. However, flavanone aglycones like naringenin and hesperetin were unique to GQP.

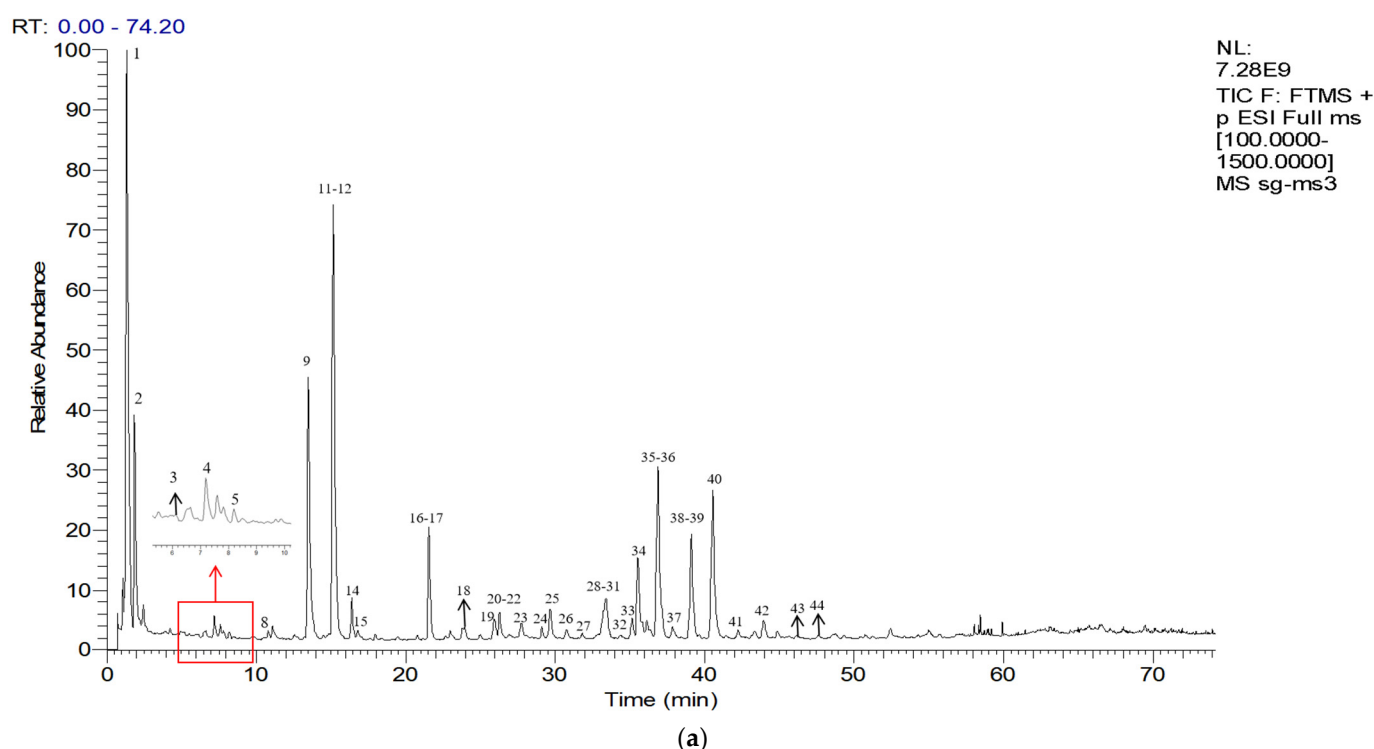


Figure 4. Cont.

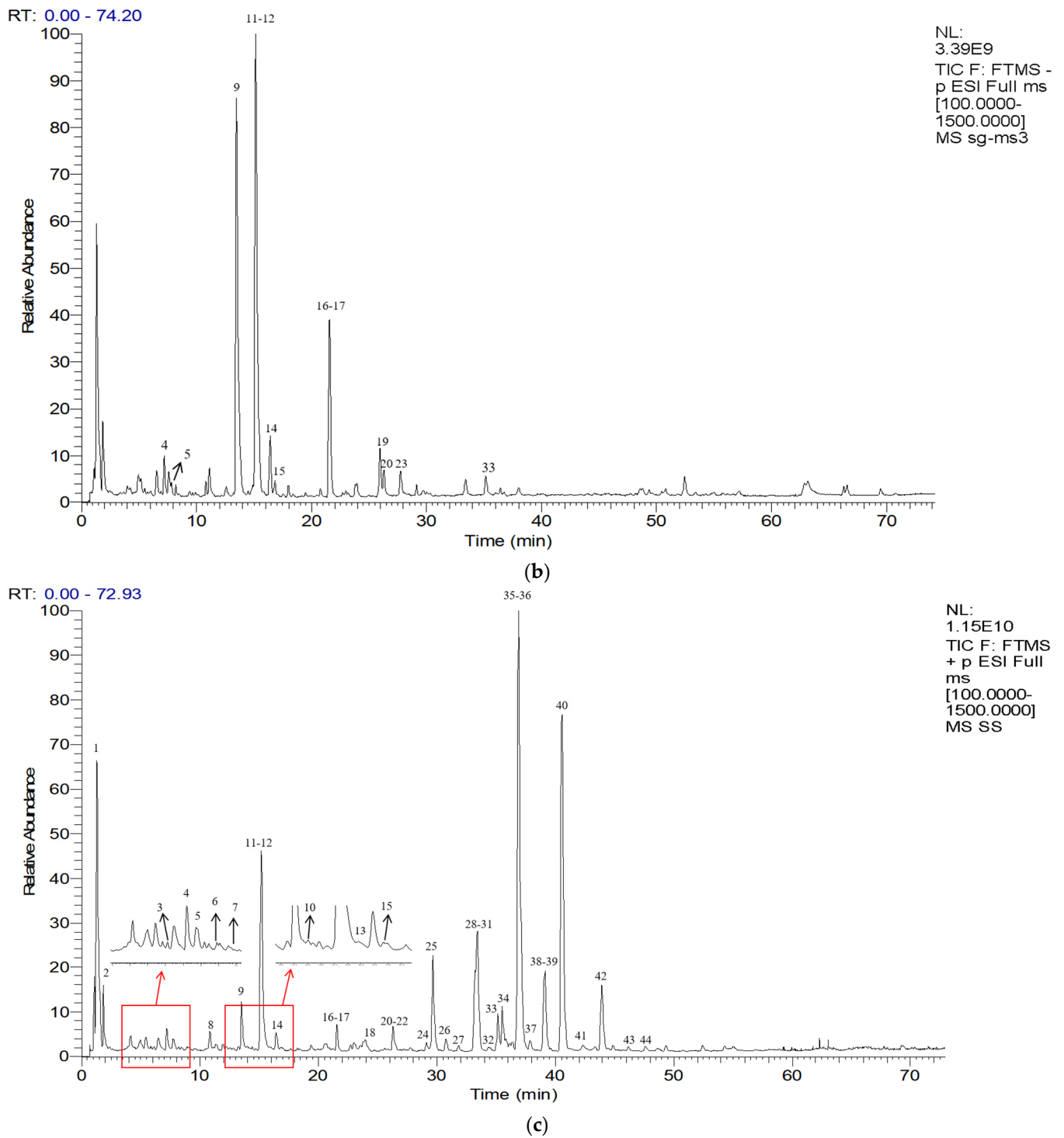


Figure 4. Cont.

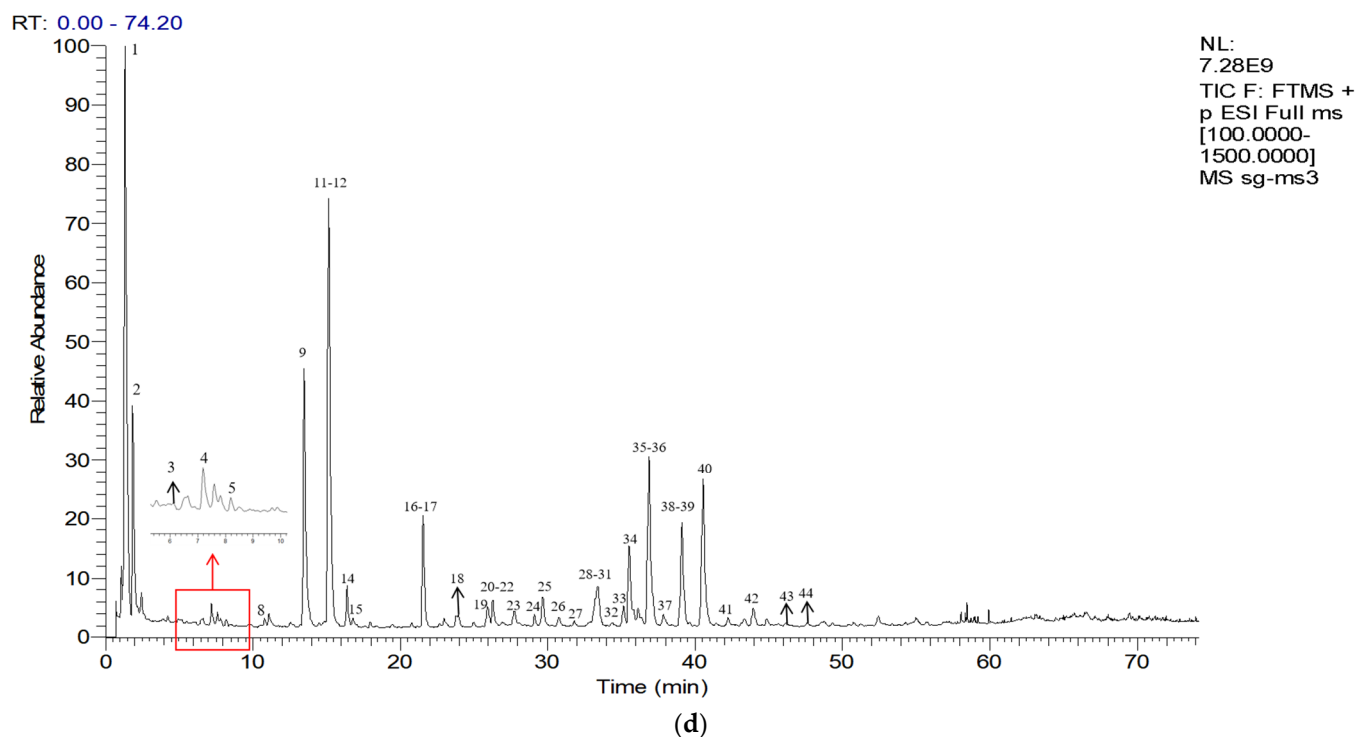


Figure 4. The basic peak chromatograms of CRPV in the positive ion mode and negative ion mode: GQP in positive ion mode (a); GQP in negative ion mode (b); SHQP in positive ion mode (c); SHQP in negative ion mode (d).

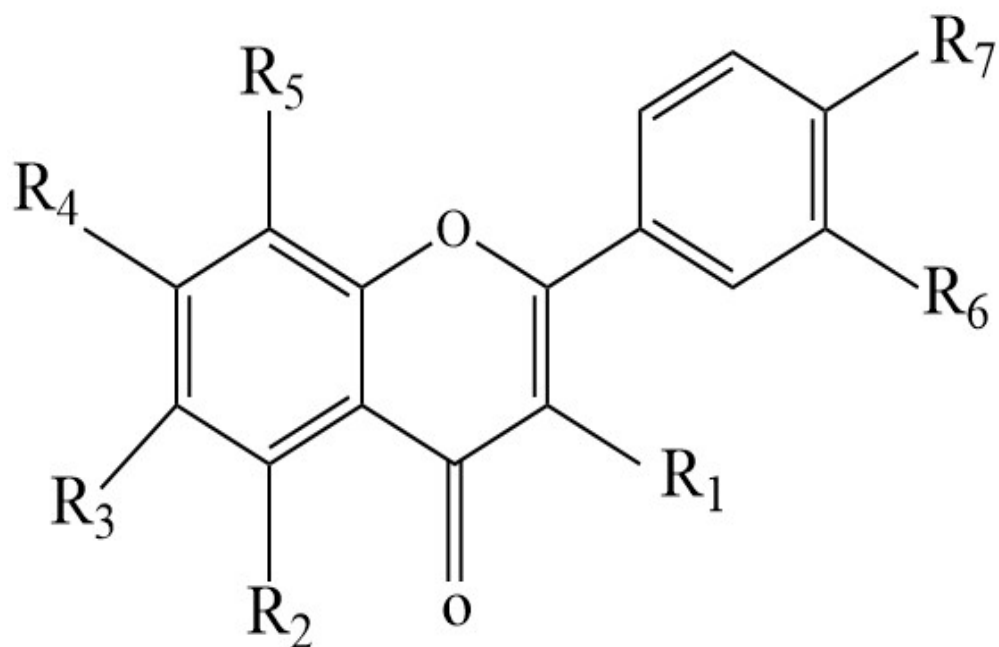


Figure 5. The structure of flavone.

Table 3. Identification of the chemical compounds of CRPV by UHPLC-Q-Exactive Orbitrap-MS.

| Compound/Peak Number | Identification | Molecular Formula | Retention Time (min) | [M + H] ⁺ (m/z) (Error, ppm) | [M – H] [–] (m/z) (Error, ppm) | Fragment Ions in the Positive Ion Mode (m/z) ^b | Fragment Ions in the Negative Ion Mode (m/z) ^b | Belongs to Medicine |
|-----------------------------|--|---|----------------------|---|---|---|---|---------------------|
| Flavone-C-glycosides | | | | | | | | |
| 3 | Luteolin-6,8-di-C-glucoside _c | C ₂₇ H ₃₀ O ₁₆ | 6.12 | 611.15961 (–1.72) | ND | 557.12787 [M + H-OCH ₂ CH ₃] ⁺ , 473.10663 [M + H-C ₄ H ₈ O ₄ -H ₂ O] ⁺ , 353.06503 [M + H-2C ₄ H ₈ O ₄ -H ₂ O] ⁺ | ND | G/S |
| 4 | Victern-2 (apigenin-6,8-di-C-glucoside) _c | C ₂₇ H ₃₀ O ₁₅ | 7.21 | 595.16406 (–2.834) | 593.15009 (–0.011) | 457.11102 [M + H-C ₄ H ₈ O ₄ -H ₂ O] ⁺ | ND | G/S |
| 5 | Chrysoeriol-6,8-C-glucoside _c | C ₂₈ H ₂₂ O ₁₆ | 7.72 | 625.17480 (–2.417) | 623.16058 (–0.13) | 487.11911 [M + H-C ₄ H ₈ O ₄ -H ₂ O] ⁺ , 367.08112 [M + H-2C ₄ H ₈ O ₄ -H ₂ O] ⁺ | 503.12042 [M – H-C ₄ H ₈ O ₄] [–] , 413.08749 [M – H-C ₄ H ₈ O ₄ -C ₃ H ₆ O ₃] [–] , 383.07684 [M – H-2C ₄ H ₈ O ₄] [–] | G/S |
| 6 | Luteolin-6-C-glucoside _c | C ₂₁ H ₂₀ O ₁₁ | 9.04 | 449.10727 (–1.264) | 447.09268 (1.101) | 413.08545 [M + H-2H ₂ O] ⁺ , 395.07538 [M + H-3H ₂ O] ⁺ , 329.06519 [M + H-C ₄ H ₈ O ₄] ⁺ , 299.05475 [M + H-C ₈ H ₆ O ₃] ⁺ | ND | S |
| 7 | Orientin _c | C ₂₁ H ₂₀ O ₁₁ | 9.52 | 449.10687 (–2.155) | ND | 431.09659 [M + H-H ₂ O] ⁺ , 413.08609 [M + H-2H ₂ O] ⁺ , 383.07559, 353.06506, 329.06506, 311.05478, 299.05450 | ND | S |
| Flavone-O-glycosides | | | | | | | | |
| 8 | Eriodictyol-7-O-rutinoside _c | C ₂₇ H ₃₂ O ₁₅ | 10.83 | 597.17963 (–1.767) | 597.17963 (–1.767) | 289.07040, 355.08051, 195.02887, 153.01813 | ND | G/S |
| 10 | Rhoifolin _c | C ₂₇ H ₃₀ O ₁₄ | 14.01 | 579.16992 (–1.575) | 577.147 (0.257) | 433.11099 [M + H-Rha] ⁺ , 271.05981 [M + H-Glc-Rha] ⁺ , 153.01849, 85.02903 | 269.04529 [M – H-Glc-Rha] [–] | S |

Table 3. Cont.

| Compound/Peak Number | Identification | Molecular Formula | Retention Time (min) | [M + H] ⁺ (<i>m/z</i>) (Error, ppm) | [M – H] [–] (<i>m/z</i>) (Error, ppm) | Fragment Ions in the Positive Ion Mode (<i>m/z</i>) ^b | Fragment Ions in the Negative Ion Mode (<i>m/z</i>) ^b | Belongs to Medicine |
|-------------------------------|---|---|----------------------|--|--|--|--|---------------------|
| 14 | 3-Hydroxy-3-methyl-5-oxo-5-[[[(2R,3S,4S,5R,6S)-3,4,5-trihydroxy-6-[2-methoxy-4-(5,7,8-trihydroxy-6-methoxy-4-oxochromen-2-yl)phenoxy]oxan-2-yl]methoxy]pentanoic acid/2-(3-Methoxy-4-hydroxyphenyl)-3-[6-O-(3,5-dihydroxy-3-methyl-5-oxopentanoyl)-beta-D-glucopyranosyloxy]-5,7-dihydroxy-8-methoxy-4H-1-benzopyran-4-one ^c | C ₂₉ H ₃₂ O ₁₇ | 16.44 | 653.16907 (–2.156) | 651.15558 (0.007) | 347.07596, 332.05252, 301.03387, 187.05991, 145.04945, 127.03915, 85.02909 | 286.04791, 151.00246 | G/S |
| 15 | Tormaloside ^c | C ₂₈ H ₃₀ O ₁₆ | 16.84 | 623.15985 (–1.302) | 621.64514 (–0.208) | 317.06540 | 315.06540 [M – H-144-162] [–] , 271.02466, 151.00233 | G/S |
| Flavanone-O-glycosides | | | | | | | | |
| 9 | Narirutin ^{a,c} | C ₂₇ H ₃₂ O ₁₄ | 13.51 | 581.18439 (–2.092) | 579.17035 (–0.832) | 273.07533 [M + H-Glc-Rha] ⁺ , 195.02816, 153.01816, 85.02905 | 271.06091 [M – H-Glc-Rha] [–] , 151.00253 | G/S |
| 12 | Hesperidin ^{a,c} | C ₂₈ H ₃₄ O ₁₅ | 15.18 | 611.19501 (–2.037) | 609.18109 (–0.503) | 303.08820 [M + H-Glc-Rha] ⁺ , 263.05466, 219.02869, 111.04427, 85.02897 | 301.07141 [M – H-Glc-Rha] [–] , 286.04776 | G/S |
| 16 | Didymin ^c | C ₂₈ H ₃₄ O ₁₄ | 21.57 | 595.20013 (–3.364) | 593.18616 (–0.543) | 287.09140, 153.0204 [M + H-Glc-Rha-C ₉ H ₁₀ O] ⁺ , 129.05472, 111.04424, 85.02905 | 285.07639 [M – H-Glc-Rha] [–] | G/S |

Table 3. Cont.

| Compound/Peak Number | Identification | Molecular Formula | Retention Time (min) | [M + H] ⁺ (m/z) (Error, ppm) | [M – H] [–] (m/z) (Error, ppm) | Fragment Ions in the Positive Ion Mode (m/z) ^b | Fragment Ions in the Negative Ion Mode (m/z) ^b | Belongs to Medicine |
|----------------------------|--|---|----------------------|---|---|--|---|---------------------|
| 20 | Melitidin ^c | C ₃₃ H ₄₀ O ₁₈ | 26.34 | 725.22607 (–3.682) | 723.21222 (–0.788) | 419.13303 | ND | G/S |
| Flavanone aglycones | | | | | | | | |
| 11 | Homoeriodictyol ^c | C ₁₆ H ₁₄ O ₆ | 15.19 | 303.08502 (–4.472) | 301.07068 (0.051) | 153.01822 [M + H-C ₉ H ₁₀ O ₂] ⁺ | 286.04791 [M – H-CH ₃] [–] , 151.00233 [M – H-C ₉ H ₁₀ O ₂] [–] | G/S |
| 17 | Isosakuranetin ^c | C ₁₆ H ₁₄ O ₅ | 21.57 | 287.09030 (–3.832) | 285.07590 (0.526) | 153.01819 [M + H-C ₉ H ₁₀ O] ⁺ , 133.06485, 161.05966 | 243.06580 [M – H-C ₂ H ₂ O] [–] , 151.00258 [M – H-C ₉ H ₁₀ O] [–] | G/S |
| 19 | Naringenin ^c | C ₁₅ H ₁₂ O ₅ | 25.93 | 273.07462 (–2.380) | 271.06021 (0.406) | 153.01817 [M + H-C ₈ H ₈ O] ⁺ , 171.02881, 147.03499, 119.04930, 91.05465, 67.01865 | 151.00258 [M – H-C ₈ H ₈ O] [–] , 119.04896 [M – H-C ₇ H ₄ O ₄] [–] , 107.01255 [M – H-C ₈ H ₈ O-CO ₂] [–] | G |
| 23 | Hesperetin ^c | C ₁₆ H ₁₄ O ₆ | 27.73 | 303.08527 (–3.447) | 301.07068 (0.051) | 153.01822 [M + H-C ₉ H ₁₀ O ₂] ⁺ , 287.07544, 219.06482, 171.02875, 177.05461 | ND | G |
| PMFs | | | | | | | | |
| 13 | Piloin ^c | C ₁₇ H ₁₄ O ₆ | 15.60 | 315.08542 (–0.895) | ND | 300.06253 [M + H-CH ₃] ⁺ , 285.03963 [M + H-2CH ₃] ⁺ , 136.01561 [M + H-CH ₃ -C ₉ H ₈ O ₃] ⁺ | ND | S |
| 21 | Monohydroxy-trimethoxyflavone ^c | C ₁₈ H ₁₆ O ₆ | 26.55 | 329.10101 (–2.901) | ND | 314.07339 [M + H-CH ₃] ⁺ , 299.05457 [M + H-2CH ₃] ⁺ , 268.07254, 181.01285, 153.01811 | ND | G/S |
| 22 | 7-Hydroxy-3,5,6,8-tetramethoxyflavone ^c | C ₁₉ H ₁₈ O ₇ | 26.59 | 359.11145 (–3.006) | ND | 344.08826 [M + H-CH ₃] ⁺ , 301.07016 [M + H-2CH ₃ -CO] ⁺ , 298.08319 | ND | G/S |

Table 3. Cont.

| Compound/Peak Number | Identification | Molecular Formula | Retention Time (min) | [M + H] ⁺ (m/z) (Error, ppm) | [M – H] [–] (m/z) (Error, ppm) | Fragment Ions in the Positive Ion Mode (m/z) ^b | Fragment Ions in the Negative Ion Mode (m/z) ^b | Belongs to Medicine |
|----------------------|--|--|----------------------|---|---|---|---|---------------------|
| 24 | 7-Hydroxy-3',4',5,6,8-pentamethoxyflavone _c | C ₂₀ H ₂₀ O ₈ | 29.10 | 389.12201 (–2.786) | ND | 374.09921 [M + H-CH ₃] ⁺ , 359.07571 [M + H-2CH ₃] ⁺ , 341.06537 [M + H-2CH ₃ -H ₂ O] ⁺ | ND | G/S |
| 25 | Isosinensetin (3',4',5,7,8-Pentamethoxyflavone) _c | C ₂₀ H ₂₀ O ₇ | 29.66 | 373.12717 (–2.705) | ND | 343.08087 [M + H-2CH ₃] ⁺ , 315.08609 [M + H-2CH ₃ -CO] ⁺ | ND | G/S |
| 26 | 3'-Hydroxy-4',5,6,7,8-Pentramethoxyflavone _c | C ₂₀ H ₂₀ O ₈ | 30.77 | 389.12219 (–2.786) | ND | 374.09912 [M + H-CH ₃] ⁺ , 359.07562 [M + H-2CH ₃] ⁺ | ND | G/S |
| 27 | 3,4',5,7-Tetramethoxyflavone _c | C ₁₉ H ₁₈ O ₆ | 31.86 | 343.11694 (–1.967) | ND | 327.08597 [M + H-CH ₄] ⁺ , 328.09256 [M + H-CH ₃] ⁺ , 299.09109 [M + H-CH ₄ -CO] ⁺ , 163.03397 | ND | G/S |
| 28 | Monohydroxy-hexamethoxyflavone _c | C ₂₁ H ₂₂ O ₉ | 32.74 | 419.13324 (–0.999) | ND | 404.10974 [M + H-CH ₃] ⁺ , 389.08646 [M + H-2CH ₃] ⁺ | ND | G/S |
| 29 | 5-Hydroxy-3',4',7,8-tetramethoxyflavone _c | C ₁₉ H ₁₈ O ₇ | 33.12 | 359.11148 (–2.922) | ND | 197.0105 [M + H-C ₁₀ H ₁₀ O ₂] ⁺ , 169.0165 [M + H-C ₁₀ H ₁₀ O ₂ -CO] ⁺ | ND | G/S |
| 30 | Sinensetin (3',4',5,6,7-Pentramethoxyflavone) _c | C ₂₀ H ₂₀ O ₇ | 33.22 | 373.12723 (–2.545) | ND | 357.09563 [M + H-CH ₄] ⁺ , 343.08081 [M + H-2CH ₃] ⁺ | ND | G/S |
| 31 | 4',5,6,7-Tetramethoxyflavone | C ₁₉ H ₁₈ O ₆ | 33.43 | 343.11673 (–2.579) | ND | 328.09363 [M + H-CH ₃] ⁺ , 317.07031, 285.07556, 181.01324, 153.01805 | ND | G/S |
| 32 | 3',4',5,7,8-Pentamethoxyflavanone _c | C ₂₀ H ₂₂ O ₇ | 34.47 | 375.14322 (–0.609) | ND | 211.05995 [M + H-C ₁₀ H ₁₀ O ₂] ⁺ , 196.03661 [M + H-C ₁₀ H ₁₀ O ₂ -CH ₃] ⁺ , 168.04150 | ND | G/S |

Table 3. Cont.

| Compound/Peak Number | Identification | Molecular Formula | Retention Time (min) | [M + H] ⁺ (<i>m/z</i>) (Error, ppm) | [M – H] [–] (<i>m/z</i>) (Error, ppm) | Fragment Ions in the Positive Ion Mode (<i>m/z</i>) ^b | Fragment Ions in the Negative Ion Mode (<i>m/z</i>) ^b | Belongs to Medicine |
|----------------------|---|--|----------------------|--|--|---|--|---------------------|
| 35 | Nobiletin (3',4',5,6,7,8-hexamethoxyflavone) _{a,c} | C ₂₁ H ₂₂ O ₈ | 36.90 | 403.13779 (–2.367) | ND | 373.09137 [M + H-2CH ₃] ⁺ , 355.08060 [M + H-3CH ₃] ⁺ , 327.08591, 312.0705, 301.07031, 211.02361, 183.02884 | ND | G/S |
| 36 | 4',5,7,8-Teramethoxyflavone _c | C ₁₉ H ₁₈ O ₆ | 37.23 | 343.11685 (–2.229) | ND | 313.07028 [M + H-2CH ₃] ⁺ , 327.08560 [M + H-CH ₄] ⁺ | ND | G/S |
| 37 | Dihydroxy-tetramethoxyflavone _c | C ₁₉ H ₁₈ O ₈ | 37.86 | 375.10706 (–1.024) | ND | 360.08340 [M + H-CH ₃] ⁺ , 345.06018 [M + H-2CH ₃] ⁺ , 327.04971 [M + H-2CH ₃ -H ₂ O] ⁺ | ND | G/S |
| 39 | 3,5,6,7,8,3',4'-Hexamethoxyflavone _c | C ₂₂ H ₂₄ O ₉ | 39.14 | 433.14835 (–2.213) | ND | 418.12482 [M + H-CH ₃] ⁺ , 403.10187 [M + H-2CH ₃] ⁺ , 385.09146 [M + H-2CH ₃ -H ₂ O] ⁺ , 345.05917 [M + H-4CH ₃ -CO] ⁺ , 211.02190, 165.05423 | ND | G/S |
| 40 | Tangeretin (4',5,6,7,8-Pentamethoxyflavone) _{a,c} | C ₂₀ H ₂₀ O ₇ | 40.56 | 373.12738 (–2.143) | ND | 358.10428, 343.08102 [M + H-2CH ₃] ⁺ , 297.07553, 183.02886, 135.04411 | ND | G/S |
| 41 | Monohydroxy-tetramethoxyflavone _c | C ₁₉ H ₁₈ O ₇ | 42.31 | 359.11206 (–1.307) | ND | 343.08096, 315.08582, 298.08322, 164.08301 | ND | G/S |
| 42 | 5-Hydroxy-6,7,8,3',4'-Pentamethoxyflavone _c | C ₂₀ H ₂₀ O ₈ | 43.91 | 389.12213 (–2.477) | ND | 374.09550, 359.07574 [M + H-2CH ₃] ⁺ , 341.06528, 215.01813, 197.0119 [M + H-C ₁₀ H ₁₂ O ₂ -2CH ₃] ⁺ | ND | G/S |

Table 3. Cont.

| Compound/Peak Number | Identification | Molecular Formula | Retention Time (min) | [M + H] ⁺ (m/z) (Error, ppm) | [M – H] [–] (m/z) (Error, ppm) | Fragment Ions in the Positive Ion Mode (m/z) ^b | Fragment Ions in the Negative Ion Mode (m/z) ^b | Belongs to Medicine |
|----------------------|--|---|----------------------|---|---|--|---|---------------------|
| 43 | Natsudaïdain (3-hydroxy-3',4',5,6,7,8-Hexamethoxyflavone) ^c | C ₂₁ H ₂₂ O ₉ | 46.20 | 419.13290 (–1.810) | ND | 389.08630 [M + H-2CH ₃] ⁺ , 371.07581 [M + H-2CH ₃ -H ₂ O] ⁺ , 361.09167 | ND | G/S |
| 44 | Monohydroxy-tetramethoxyflavone ^c | C ₁₉ H ₁₈ O ₇ | 47.65 | 359.11179 (–2.0598) | ND | 344.08826 [M + H-CH ₃] ⁺ , 329.06528 [M + H-2CH ₃] ⁺ , 197.00768 | ND | G/S |
| Alkaloids | | | | | | | | |
| 1 | Stachydrine ^c | C ₇ H ₁₃ NO ₂ | 1.30 | 144.10161 | ND | 102.05531, 84.08133, 58.06592 | ND | G/S |
| 2 | Synephrine ^{a,c} | C ₉ H ₁₃ NO ₂ | 1.84 | 168.10179 | ND | 135.06801 [M + H-H ₂ O-CH ₃] ⁺ , 119.04944 [M + H-H ₂ O-CH ₃ NO ₂] ⁺ , 107.04957 [M + H-H ₂ O-CH ₃ -CO] ⁺ , 91.05482, 81.07052 | ND | G/S |
| 18 | CitrusinIII ^c | C ₃₆ H ₅₃ N ₇ O ₉ | 23.97 | 728.39557 (–2.722) | ND | 700.40399 [M + H-CO] ⁺ , 587.31830, 474.23471 | ND | G/S |
| Limonoids | | | | | | | | |
| 33 | Limonin ^c | C ₂₆ H ₃₀ O ₈ | 35.15 | 471.20053 (–1.728) | 469.18555 (–0.307) | 425.19559 [M + H-H ₂ O] ⁺ , 367.19043 [M + H-CH ₂ O ₂ -2CH ₃ -H ₂ O] ⁺ , 161.05972 | ND | G/S |
| 38 | Nomilin ^c | C ₂₈ H ₃₄ O ₉ | 39.03 | 515.22668 (–1.706) | ND | 469.22083 [M + H-CH ₂ O ₂] ⁺ , 411.21735 [M + H-CH ₂ O ₂ -2CH ₃ -H ₂ O] ⁺ , 161.05966 | ND | G/S |

Table 3. Cont.

| Compound/Peak Number | Identification | Molecular Formula | Retention Time (min) | [M + H] ⁺ (m/z) (Error, ppm) | [M – H] [–] (m/z) (Error, ppm) | Fragment Ions in the Positive Ion Mode (m/z) ^b | Fragment Ions in the Negative Ion Mode (m/z) ^b | Belongs to Medicine |
|------------------------|---|---|----------------------|---|---|---|---|---------------------|
| Other compounds | | | | | | | | |
| 14 | 2-(carbamoylamino)ethyl-[5-(dimethylamino)pentyl]-methylpropylazanium/diethyl-[[[2-methyl-3-[1-(methylamino)butan-2-ylamino]propanoyl]amino]methyl]azanium ^c | C ₁₄ H ₃₃ ON ₄ | 35.54 | 274.27328 (–2.066) | ND | 256.26324, 106.08664, 88.07628 | ND | G/S |

G: Geqingpi belongs to CRPV; S: Sihuaqingpi belongs to CRPV; ^a Confirmation in comparison with authentic standards.; ^b Glc = glucose moiety, Rha = rhamnose moiety, ND: Not detected; ^c Confirmation in comparison with literature.

Table 4. Compounds with the flavone structure.

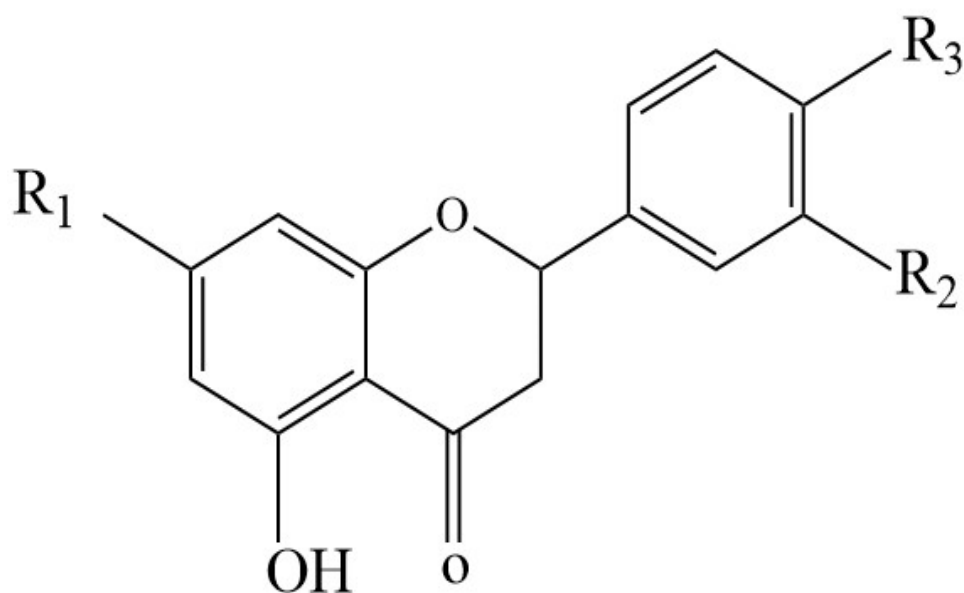
| Name | R1 | R2 | R3 | R4 | R5 | R6 | R7 |
|---|------------------|------------------|------------------|------------------|------------------|------------------|------------------|
| Luteolin-6,8-di-C-glucoside | H | OH | Glc | OH | Glc | OH | OH |
| Victern-2 (apigenin-6,8-di-C-glucoside) | H | OH | Glc | OH | Glc | H | OH |
| Chrysoeriol-6,8-C-glucoside | H | OH | Glc | OH | Glc | OCH ₃ | OH |
| Rhoifolin | H | OH | H | ONeo | H | H | OH |
| Isosinensetin (3',4',5,7,8-Pentamethoxyflavone) | OCH ₃ | H | OCH ₃ | OCH ₃ | OCH ₃ | OCH ₃ | OCH ₃ |
| Sinensetin (5,6,7,3',4'-Pentramethoxyflavone) | OCH ₃ | OCH ₃ | OCH ₃ | H | OCH ₃ | OCH ₃ | OCH ₃ |
| Nobiletin (5,6,7,8,3',4'-hexamethoxyflavone) | OCH ₃ | OCH ₃ | OCH ₃ | OCH ₃ | OCH ₃ | OCH ₃ | OCH ₃ |
| Tangeretin (5,6,7,8,4'-Pentamethoxyflavone) | OCH ₃ | OCH ₃ | OCH ₃ | OCH ₃ | H | H | OCH ₃ |
| 3,5,6,7,8,3',4'-Hexamethoxyflavone | H | OCH ₃ | OCH ₃ | OCH ₃ | OCH ₃ | OCH ₃ | OCH ₃ |

Glc = glucose, Neo = neohesperidoside.

Table 5. Compounds with the flavanone structure.

| Name | R1 | R2 | R3 |
|-----------------|------|------------------|------------------|
| Narirutin | ORut | H | OH |
| Hesperidin | ORut | OH | OCH ₃ |
| Homoeriodictyol | OH | OCH ₃ | OH |
| Isosakuranetin | OH | H | OCH ₃ |
| Didymin | ONeo | H | OCH ₃ |
| Naringenin | OH | H | OH |
| Hesperetin | OH | OH | OCH ₃ |

Rut = rutinoside, Neo = neohesperidoside.

**Figure 6.** The structure of flavanone.

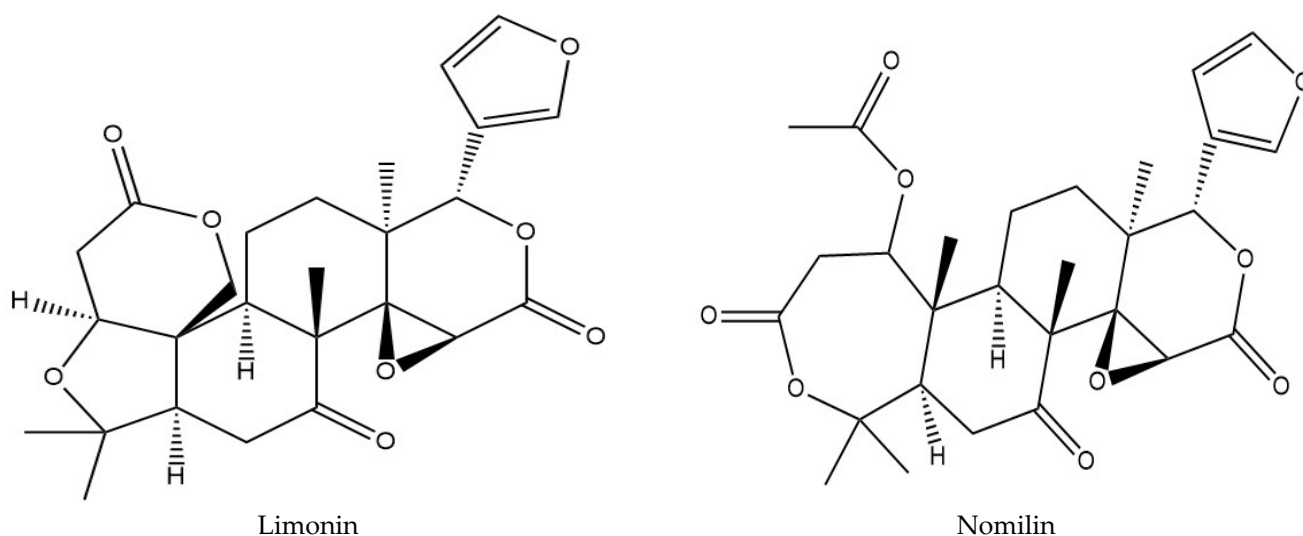


Figure 7. The structures of Limonin and Nomilin.

2.4.1. Analysis of Flavonoids

In this study, we identified 44 major components including 5 flavone-C-glycosides, 4 flavone-O-glycosides, 4 flavanone-O-glycosides, 4 flavanone aglycones, 21 PMFs, 3 alkaloids, 2 limonoids, and 1 other compound from the CRPV samples. Consistent with the previously reported results [31], the retro Diels–Alder (rDA) reaction often exists in the cracking process of most flavonoids.

Analysis of Flavonoid-O-Glycosides

Flavonoid-O-glycosides are common flavonoid compounds commonly found in citrus fruits, and are linked to rutinose or neohesperidose via the C-7 hydroxyl group, which links the disaccharide to the aglycone [32,33]. Based on previous reports [34–37], we identified and tentatively characterized four flavone-O-glycosides (compounds 8, 10, 14, and 15) and four flavanone-O-glycosides (compounds 9, 12, 16, and 20). For instance, compared with reference standards, we unambiguously identified compounds 9 and 12 as narirutin and hesperidin, respectively. Hesperidin showed a quasi-molecular ion $[M + H]^+$ at m/z of 611.19501 ($C_{28}H_{34}O_{15}$), due to the continuous loss of a glucose (162 Da) and a rhamnose (146 Da), thereby giving characteristic product ions at m/z of 303.08820. Narirutin gave an $[M + H]^+$ signal at m/z of 581.08439 ($C_{27}H_{32}O_{14}$), and its fragmentation pattern shared similarity with hesperidin, which generated MS/MS ions at m/z of 273.07533 $[M + H-Glc-Rha]^+$.

Analysis of Flavonoid-C-Glycosides

Fragmentations in most flavonoid-C-glycosides were based on the aglycones of flavones [38]. In the MS/MS spectra, the main product ion of flavone-C-glycosides usually occurred in the glycosyl moiety, which was generated by the loss of water molecule(s) and the glycosidic methylol group as formaldehyde [39]. According to previous reports [34–37], the product ions $[M + H-n18Da]^+$ are diagnostic ions, while the other two fragments, $[M-H-90Da]^-$ and $[M-H-120Da]^-$, revealed that a C-glycoside was connected with hexose units. In the present study, we tentatively identified five flavone-C-glycosides (compounds 3, 4, 5, 6, and 7) in CRPV, in which compounds 6 and 7 belong to SHQP. For example, compound 3 showed a quasi-molecular ion $[M + H]^+$ at m/z of 611.15961 ($C_{27}H_{30}O_{16}$), which generated MS/MS ions at m/z of 557.12787 $[M + H-OCH_3-H_2O]^+$, 473.10663 $[M + H-C_4H_8O_4-H_2O]^+$, and 353.06503 $[M + H-2C_4H_8O_4-H_2O]^+$. Compound 4 exhibited a quasi-molecular ion $[M + H]^+$ at m/z of 595.16406 ($C_{27}H_{30}O_{15}$), which generated MS/MS ions at 457.11102 $[M + H-C_4H_8O_4-H_2O]^+$. Compound 5 displayed a quasi-

molecular ion $[M + H]^+$ at m/z of 625.17480 ($C_{28}H_{22}O_{16}$), which generated MS/MS ions at m/z of 487.11911 $[M + H - C_4H_8O_4 - H_2O]^+$ and 367.08112 $[M + H - 2C_4H_8O_4 - H_2O]^+$. Compound **6** exhibited a quasi-molecular ion $[M + H]^+$ at m/z of 449.10727 ($C_{21}H_{20}O_{11}$), which generated MS/MS ions at 413.08545 $[M + H - 2H_2O]^+$ and 395.07538 $[M + H - 3H_2O]^+$. Compound **7** presented a quasi-molecular ion $[M + H]^+$ at m/z of 449.10727 ($C_{21}H_{20}O_{11}$), which generated MS/MS ions at m/z of 413.08545 $[M + H - 2H_2O]^+$ and 395.07538 $[M + H - 3H_2O]^+$. On comparing with the flavonoid-C-glycosides in the existing literature, we tentatively identified compounds **3**, **4**, **5**, **6**, and **7** as luteolin-6,8-di-C-glucoside, victern-2, chrysoeriol-6,8-C-glucoside, luteolin-6-C-glucoside, and orientin, respectively.

Analysis of PMFs

PMFs are almost exclusively found in citrus species [40]. They have the same aglycon structure; the difference lies in the number and position of the hydroxyl groups (-OH) and/or methoxy groups (-OCH₃) connected to the A, B, and C rings of the aglycon. Furthermore, the diagnostic ions of PMFs are $[M + H - nCH_3]^+$, $[M + H - 2CH_3 - H_2O]^+$, $[M + H - 2CH_3 - CO]^+$, etc. [41]. By comparison with elution times and MS/MS data from previous reports [34,35], we screened 21 PMFs in CRPV. For example, by comparing with the reference standards, we identified compounds **35** and **40** as nobiletin and tangeretin, respectively. Nobiletin exhibited a quasi-molecular ion $[M + H]^+$ at m/z of 403.13779 ($C_{18}H_{16}O_7$) and displayed secondary fragments at m/z of 373.09137 $[M + H - 2CH_3]^+$. Tangeretin exhibited a quasi-molecular ion $[M + H]^+$ at m/z of 373.12783 ($C_{20}H_{20}O_7$) and displayed secondary fragments at m/z of 328.0622 $[M + H - CH_3]^+$ and 343.08102 $[M + H - 2CH_3]^+$. Compound **39** presented a quasi-molecular ion $[M + H]^+$ at m/z 433.14835 ($C_{22}H_{24}O_9$), which generated MS/MS ions at m/z of 418.12482 $[M + H - CH_3]^+$, 403.10187 $[M + H - 2CH_3]^+$, and 385.09146 $[M + H - 2CH_3 - H_2O]^+$. On comparing with the existing literature, we tentatively identified compound **39** as 3,5,6,7,8,3',4'-Hexamethoxyflavone.

2.4.2. Analysis of Other Compounds

Compounds **33** and **38** showed a quasi-molecular ion $[M + H]^+$ at m/z of 471.20053 ($C_{26}H_{30}O_8$) and 515.22668 ($C_{28}H_{34}O_9$), respectively. The characteristic ions of these compounds were usually generated by the loss of H₂O, CO, and CO₂, and displayed secondary fragments at m/z of 425.19559 $[M + H - H_2O]^+$, 367.19043 $[M + H - CH_2O_2 - 2CH_3 - H_2O]^+$, 469.22083 $[M + H - CH_2O_2]^+$, and 411.21735 $[M + H - CH_2O_2 - 2CH_3 - H_2O]^+$. When compared with the previous reports, compounds **33** and **38** were identified as limonin and nomilin [34,35].

2.5. Statistical Analysis

We applied different statistical analyses like the similarity analysis, PCA analysis, and OPLS-DA analysis, based on the FT-IR information. Similarity analysis between samples was calculated as Euclidean distance, and the final result is shown in Table 6. The larger the value, the higher the similarity between the samples, while the smaller the value, the lower the similarity between the samples. The similarity value between the GQP varieties is 1.00, and the similarity between the SHQP varieties is also 1.00. However, the similarity value between GQP and SHQP is 0.65~0.66. This means that there are large differences between GQP and SHQP.

We established a PCA model and an unsupervised pattern recognition technique with $R^2(X)$ (cum) = 0.748 and Q^2 (cum) = 0.588. The final PCA score scatter plot and bi-plot are shown in Figure 8a,b. As shown in Figure 8a, we separated the samples into distinct groups. GQP and SHQP were clustered together; as well as being visible to the naked eye in Figure 8b, this feature indicates that samples fell into two classes; different infrared peaks had different effects between GQP and SHQP. The infrared peaks numbered 7, 16, 2, 8, and 3 had a greater impact on the clustering of SHQP, while the rest had a greater impact on the clustering of GQP. A clear separation between GQP and SHQP was achieved, indicating the significant differences between these two species.

Table 6. Similarity analysis of GQP and SHQP.

| Sample Number | G1 | G2 | G3 | G4 | G5 | G6 | G7 | G8 | G9 | G10 | G11 | G12 | S13 | S14 | S15 | S16 | S17 | S18 | S19 | S20 | S21 | S22 | |
|---------------|------|------|------|------|------|------|------|------|------|------|------|------|------|------|------|------|------|------|------|------|------|------|--|
| G1 | 1.00 | | | | | | | | | | | | | | | | | | | | | | |
| G2 | 1.00 | 1.00 | | | | | | | | | | | | | | | | | | | | | |
| G3 | 1.00 | 1.00 | 1.00 | | | | | | | | | | | | | | | | | | | | |
| G4 | 1.00 | 1.00 | 1.00 | 1.00 | | | | | | | | | | | | | | | | | | | |
| G5 | 1.00 | 1.00 | 1.00 | 1.00 | 1.00 | | | | | | | | | | | | | | | | | | |
| G6 | 1.00 | 1.00 | 1.00 | 1.00 | 1.00 | 1.00 | | | | | | | | | | | | | | | | | |
| G7 | 1.00 | 1.00 | 1.00 | 1.00 | 1.00 | 1.00 | 1.00 | | | | | | | | | | | | | | | | |
| G8 | 1.00 | 1.00 | 1.00 | 1.00 | 1.00 | 1.00 | 1.00 | 1.00 | | | | | | | | | | | | | | | |
| G9 | 1.00 | 1.00 | 1.00 | 1.00 | 1.00 | 1.00 | 1.00 | 1.00 | 1.00 | | | | | | | | | | | | | | |
| G10 | 1.00 | 1.00 | 1.00 | 1.00 | 1.00 | 1.00 | 1.00 | 1.00 | 1.00 | 1.00 | | | | | | | | | | | | | |
| G11 | 1.00 | 1.00 | 1.00 | 1.00 | 1.00 | 1.00 | 1.00 | 1.00 | 1.00 | 1.00 | 1.00 | | | | | | | | | | | | |
| G12 | 1.00 | 1.00 | 1.00 | 1.00 | 1.00 | 1.00 | 1.00 | 1.00 | 1.00 | 1.00 | 1.00 | 1.00 | | | | | | | | | | | |
| S13 | 0.66 | 0.66 | 0.65 | 0.65 | 0.65 | 0.66 | 0.65 | 0.65 | 0.65 | 0.65 | 0.65 | 0.65 | 1.00 | | | | | | | | | | |
| S14 | 0.65 | 0.65 | 0.65 | 0.65 | 0.65 | 0.65 | 0.65 | 0.65 | 0.65 | 0.65 | 0.65 | 0.65 | 1.00 | 1.00 | | | | | | | | | |
| S15 | 0.66 | 0.65 | 0.65 | 0.65 | 0.65 | 0.65 | 0.65 | 0.65 | 0.65 | 0.65 | 0.65 | 0.65 | 1.00 | 1.00 | 1.00 | | | | | | | | |
| S16 | 0.66 | 0.66 | 0.65 | 0.65 | 0.65 | 0.65 | 0.65 | 0.65 | 0.65 | 0.65 | 0.65 | 0.65 | 1.00 | 1.00 | 1.00 | 1.00 | | | | | | | |
| S17 | 0.65 | 0.65 | 0.65 | 0.65 | 0.65 | 0.65 | 0.65 | 0.65 | 0.65 | 0.65 | 0.65 | 0.65 | 1.00 | 1.00 | 1.00 | 1.00 | 1.00 | | | | | | |
| S18 | 0.66 | 0.66 | 0.66 | 0.66 | 0.66 | 0.66 | 0.66 | 0.65 | 0.66 | 0.66 | 0.66 | 0.66 | 1.00 | 1.00 | 1.00 | 1.00 | 1.00 | 1.00 | | | | | |
| S19 | 0.65 | 0.65 | 0.65 | 0.65 | 0.65 | 0.65 | 0.65 | 0.65 | 0.65 | 0.65 | 0.65 | 0.65 | 1.00 | 1.00 | 1.00 | 1.00 | 1.00 | 1.00 | 1.00 | | | | |
| S20 | 0.66 | 0.66 | 0.65 | 0.65 | 0.66 | 0.66 | 0.65 | 0.65 | 0.66 | 0.66 | 0.65 | 0.65 | 1.00 | 1.00 | 1.00 | 1.00 | 1.00 | 1.00 | 1.00 | 1.00 | | | |
| S21 | 0.65 | 0.65 | 0.65 | 0.65 | 0.65 | 0.65 | 0.65 | 0.65 | 0.65 | 0.65 | 0.65 | 0.65 | 1.00 | 1.00 | 1.00 | 1.00 | 1.00 | 1.00 | 1.00 | 1.00 | 1.00 | | |
| S22 | 0.66 | 0.65 | 0.65 | 0.65 | 0.65 | 0.65 | 0.65 | 0.65 | 0.65 | 0.65 | 0.65 | 0.65 | 1.00 | 1.00 | 1.00 | 1.00 | 1.00 | 1.00 | 1.00 | 1.00 | 1.00 | 1.00 | |

We established the OPLS-DA model by setting GQP and SHQP as groups I and II, respectively. The OPLS-DA scores plot was established with the model parameters of R^2 (Y) = 0.999 and Q^2 (cum) = 0.997 and is shown in Figure 8c. Therefore, we confirmed the OPLS-DA model based on the FT-IR data used to separate GQP and SHQP. Since the variable importance in the projection (VIP) value reflected the contribution of each variable to the grouping, we used $VIP \geq 1$ as the threshold to filter and obtain eleven different infrared peaks related to species classification (Figure 8d). The VIP values of the infrared peaks numbered 13, 12, 11, 21, 15, 9, 17, 14, 3, and 5 were > 1 , and all these were important for distinguishing between GQP and SHQP. The permuted R^2 and Q^2 values on the left were lower than the original point on the right (Figure 8e), thus indicating that the established OPLS-DA mode has high goodness of fit and predictability.

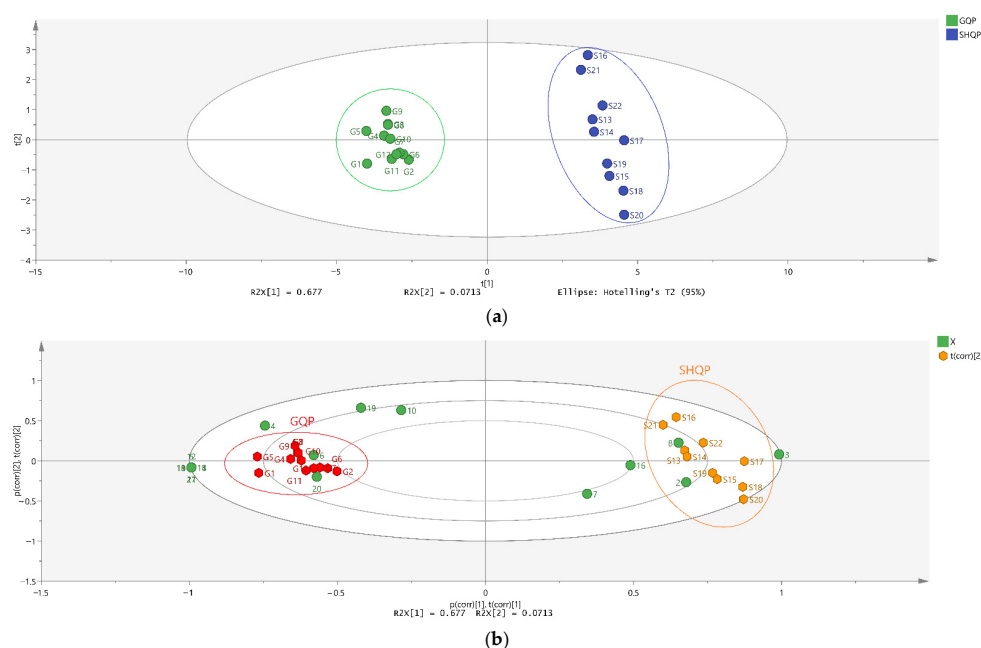


Figure 8. Cont.

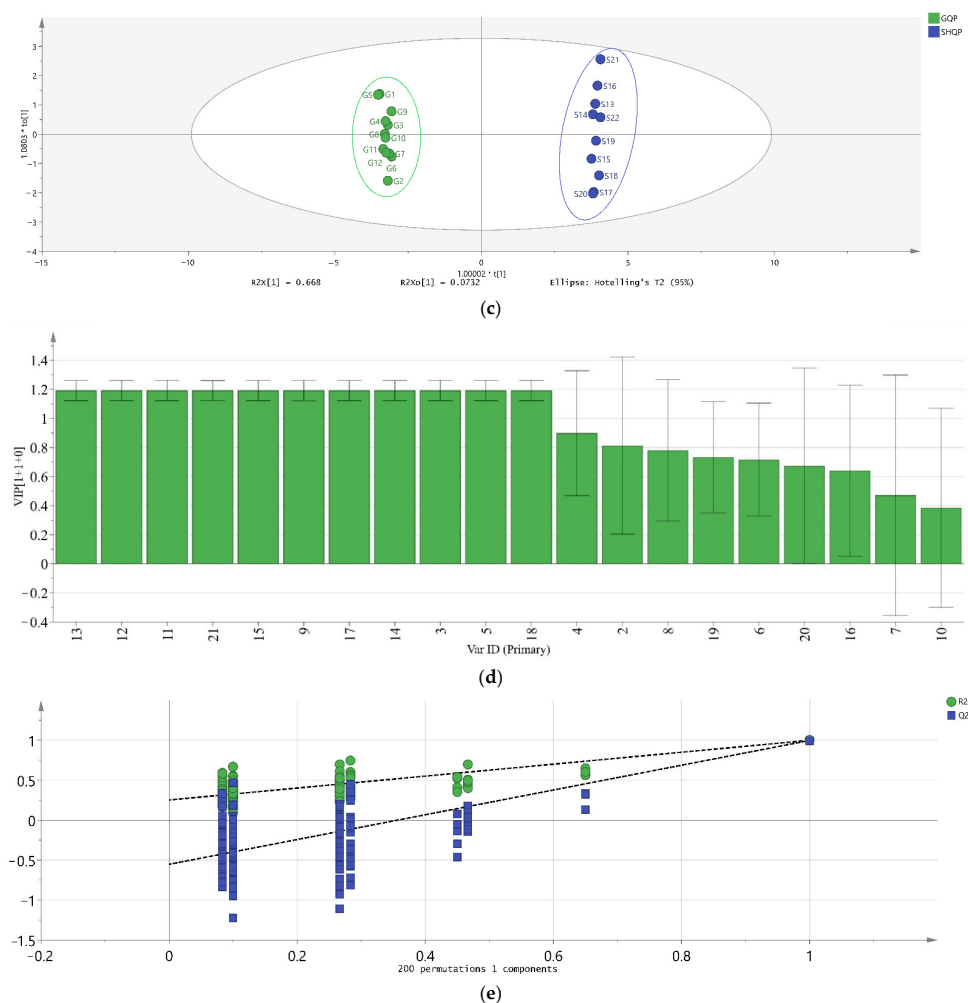


Figure 8. Score plot (a) and bi plot (b) of PCA model; score plot (c), variable importance in projection (d), and permutation test (e) of OPLS-DA model based on data of FT-IR.

3. Materials and Methods

3.1. Chemicals and Materials

Hesperidin (China National Institute for Food and Drug Control), narirutin (Chengdu Keluo Biological Technology Co., Ltd., Chengdu, China), nobiletin (Chengdu Pusi Biological Technology Co., Ltd.; Chengdu, China), tangeretin (Chengdu Pusi Biological Technology Co., Ltd.; Chengdu, China), acetonitrile (Merck Co., Kenilworth, NJ, USA), methanol (Tianjin Concord, Tianjin, China), formic acid (Nanjing Chemical Reagents Co., Nanjing, China).

Twenty-two batches of CRPV samples, comprising the GQP and SHQP, from different provinces of China, were purchased from various pharmacies and markets (Figure 9, Supporting Information Table S1). They were authenticated by Professor Feng Li (Shandong University of Traditional Chinese Medicine). According to morphological characteristics, all the samples were dried fruit or immature fruit skins of *Citrus reticulata* Blanco and its cultivars. G1–G12 were GQP, and these types of GQP were round thick slices, the surface was grayish-green or black-green, cut surface was yellow-white or light yellow-brown, densely living with most oil chambers, gas fragrance, bitter taste, and spicy. S13–S22 were SHQP, and these types of SHQP were irregular filamentous, surface grayish-green or black-green, cut surface was yellow-white or light yellow-brown, fragrance, bitter taste, and spicy.



Figure 9. Appearance characteristics of GQP (a) and SHQP (b).

3.2. Sample Preparation

Appropriate amounts of the reference standards were dissolved in methanol. The reference solutions were stored at 4 °C before use. All samples were ground into a thin powder through an 80-mesh sieve.

3.2.1. Sample Preparation for Microscopic Observation

A small amount of homogenized sample powder was accurately weighed, and an appropriate amount of chloral hydrate test solution (chloral hydrate:distilled water:glycerin 50:15:10) was added to it. The mixture was heated and permeated, then covered with the cover glass to make microscopic observations.

3.2.2. Sample Preparation for FT-IR

An appropriate amount of homogenized sample powder and potassium bromide powder were accurately weighed and dried separately in a constant temperature oven at 65 °C and 115 °C for 1.5 h, privately. Sample powder and potassium bromide (1:100) were mixed and ground under an infrared baking lamp, then pressed into flakes by a powder tablet press (Graseby Specac) for FT-IR analysis.

3.2.3. Sample Preparation for UHPLC-Q-Exactive Orbitrap-MS

An appropriate amount of homogenized sample powder (0.2 g) was accurately weighed and ultrasonically extracted with 25 mL methanol/water (50:50, *v/v*) for 45 min at room temperature. The suspension was centrifuged at 5000 rpm for 5 min to remove residue. Then, the solution was filtered through a 0.22 μm filter for analysis.

3.3. Powder Color, Microscopic Identification, and Chemical Composition Analysis

3.3.1. Power Color Determination Analysis

A high-quality COLORIMETER (NH300, ThreeNH Technology Co., Ltd., Shenzhen, China) was used to measure the powder color and obtain L^* (brightness), a^* (red-green), b^* (yellow-blue), and the total color value E^*_{ab} , which was obtained by the following formula: $E^*_{ab} = (L^2 + a^2 + b^2)^{1/2}$. The chromaticity meter used the international universal light source D65 with a standard deviation of $\Delta E^*_{ab} < 0.07$ (the average of 30 times of interval measurement after calibration of the standard whiteboard).

3.3.2. Microscopic Observation Analysis

An Olympus BX53F microscope (Olympus Life Sciences, Tokyo, Japan) with MC50 lens (Mshot, Mingmei Technology Co., Ltd., Guangzhou, China) was used to observe the

characteristic cells in CRPV. The microscope preview resolution was set as 2560×1944 ; the capture resolution was 2560×1944 ; no color enhancement (saturation default 100); no single color; no automatic white balance; color correction OFF.

3.3.3. FT-IR Analysis

The infrared spectrum of CRPV was scanned using a Frontier FT-IR spectrometer (Perkin Elmer, Waltham, MA, USA) along with an FR-DTGS detector. Scanning parameters were as follows: scanning range of $4000\text{--}400\text{ cm}^{-1}$, spectral resolution of 4 cm^{-1} , wavelength reactivity of $\pm 0.02\text{ cm}^{-1}$, wavelength accuracy of $\pm 0.1\text{ cm}^{-1}$. The interference of H_2O and CO_2 was deducted during scanning. After the processing of peak position and baseline correction, the maps and data were corrected using OMNIC 9.2 software (Thermo Nicolet Corporation, Madison, WI, USA).

3.3.4. UHPLC-Q-Exactive Orbitrap-MS Analysis

Detection was performed using a Vanquish FLEX ULTRA-high-performance liquid chromatography system and a quadrupole orbital well high-resolution mass spectrometer Q-Exactive (Thermo Fisher Scientific, Waltham, MA, USA). Chromatographic separation was performed with an ACQUITY C_{18} column ($2.1\text{ mm} \times 100\text{ mm}$, $1.8\text{ }\mu\text{m}$, $100\text{ }\text{\AA}$; Phenomenex, Torrance, CA, USA) maintained at $30\text{ }^\circ\text{C}$ with linear gradient elution using (A) water (0.01% formic acid) and (B) acetonitrile (0.01% formic acid) as the mobile phase. The optimized gradient elution procedure was as follows: 10 to 15% B (0–3 min), 15–37% B (3–30 min), 37–60% B (30–50 min), 60 to 85% B (50–65 min), and 85% B (75 min). The flow rate was 0.2 mL/min . The sample injection volume was $2\text{ }\mu\text{L}$.

MS/MS identification was performed using a high-resolution mass spectrometer equipped with an electrospray ionization (ESI) source using a quadrupole tandem electrostatic field track well. Ion mode: positive and negative ion mode; auxiliary temperature: $350\text{ }^\circ\text{C}$; auxiliary gas flow rate: 10; sheath gas flow rate: 35; atomization voltage: 3.0 kV ; capillary temperature: $350\text{ }^\circ\text{C}$; scan mode: full mass-DD MS2; scanning range: 100–1500. Sheath gas pressure auxiliary gas pressure: 30, 40, 50 arb. Nitrogen was used as an atomizer and auxiliary gas. Data were obtained using Thermo Scientific Xcalibur.

3.4. Statistical Analysis

Data obtained from the study are presented as mean \pm standard deviation (SD). The one-way ANOVA and similarity analyses were carried out using SPSS 22.0 statistical software (SPSS, Inc., Chicago, IL, USA). Principal component analysis (PCA) and orthogonal partial least squares-discriminant analysis (OPLS-DA) were performed using SIMCA 14.0 software (Umetrics, Inc., San Jose, CA, USA).

4. Results and Discussion

In this experiment, we studied 22 batches of CRPV (12 kinds of GQP and 10 kinds of SHQP) based on their powder color, microscopic cells, FT-IR analysis, and composition analysis. The color of SHQP powder was comparatively brighter, with the color of GQP and SHQP being comparatively redder and yellower, respectively. The microscopic characteristic cells of GQP mainly comprised calcium oxalate crystallization, epidermal cells of the pulp capsule, and hesperidin crystal, while those of SHQP mainly comprised tracheal, calcium oxalate crystallization, exocarp, mesocarp parenchyma, hesperidin crystal, and stoma. FT-IR analysis showed that SHQP had a higher content of carboxylic acids and its esters than GQP, whereas GQP had a higher content of polysaccharides than SHQP.

We detected 44 main components using the UHPLC-Q-Exactive Orbitrap-MS. Among them, the flavanone aglycones, naringenin and hesperetin, were the unique components of GQP. Naringenin can reduce the phosphorylation of STAT3 in the hypothalamus by regulating adipocytokines, to achieve weight loss in obese rats and treat hypertension [42]. In vitro and in vivo experiments have confirmed that naringenin can reduce hepatic lipid accumulation and attenuate the inflammation in mice by downregulating the expression of

the NLRP3 /NF- κ B signaling pathway both in Kupffer cells and hepatocytes [43]. Moreover, it can also decrease urea, creatine, and uric acid levels, thereby protecting against rat liver and kidney damage [44]. Hesperetin reportedly has both neuroprotective and memory-improving effects, and it works by reducing both the inflammatory mediators' expression and neuronal apoptosis [45,46].

Luteolin-6-C-glucoside, orientin, rhoifolin, and pilloin were unique components in SHQP. Previous literature has shown that orientin exhibits antibacterial effects and can inhibit the growth of *Staphylococcus aureus* [47]. Although both rhoifolin and pillion have shown anti-inflammatory effects, their mechanisms are different. Rhoifolin inhibits the secretion of inflammatory factors and inhibits the expression of IKK β and I κ B α in the NF- κ B signaling pathway [48,49]. Additionally, it can repair liver and kidney damage in mice with acute inflammation, treat rheumatoid arthritis, and exert anti-pancreatic cancer effects [50]. Pilloin inhibits the production of inflammatory molecules in macrophages and downregulates inflammatory cytokines, thus showing good anti-inflammatory activity both in vitro and in vivo [51]. However, we found no pharmacological studies related to luteolin-6-C-glucoside.

GQP has been reported to be mainly used for breaking Qi and resolving stagnation, while SHQP is mainly used for regulating both the liver and Qi [28]. The above studies prove that the pharmacological activities and action mechanisms of the different components in both GQP and SHQP are different. These may be the reasons for the differences in the clinical efficacy of GQP and SHQP. This research can provide a reference for the establishment of different grade standards of CRPV or establish identification methods for Chinese patent medicines with different CRPV as raw materials, while also helping with their clinical development as a precision medicine. More studies on the pharmacological efficacy should be carried out in the future, thus helping to formulate more reasonable quality standards for CRPV and guide its clinical use as a precision drug.

Supplementary Materials: The following supporting information can be downloaded at: <https://www.mdpi.com/article/10.3390/molecules27103285/s1>, Table S1: Information on *Citri Reticulatae Pericarpium Viride*.

Author Contributions: Methodology, Y.W. and W.C.; software, Y.W. and G.P.; validation, H.L. and Y.L.; resources, H.L.; data curation, Q.L., L.X. (Lewen Xiong) and L.X. (Lili Xu); writing—original draft preparation, Y.W.; writing—review and editing, Y.W., H.L., and Y.L. All authors have read and agreed to the published version of the manuscript.

Funding: This research was funded by the Key Technologies for Quality Identification and Control of Traditional Chinese Medicine Formula Granules and their Industrial Application (No.2021CXGC010511), the National Natural Science Foundation of Shandong Province (No.ZR2020MH374).

Institutional Review Board Statement: Not applicable.

Informed Consent Statement: Not applicable.

Data Availability Statement: Data is contained within the article or supplementary material.

Conflicts of Interest: The authors declare no conflict of interest.

Sample Availability: Samples are not available from the authors.

References

1. Lin, D.R. *Secrets of Treating Wounds and Bonesetting*; People's Medical Publishing House: Beijing, China, 1957.
2. Chinese Pharmacopoeia Commission. *ChP 2020*; China Medical Science Press: Beijing, China, 2020; Volume I.
3. Chen, J.M. *Correlation between Materia Medica Companion*; Ancient Chinese Medical Book Press: Beijing, China, 2008.
4. Zhang, L. *This Sutra Meets the Original*; China Traditional Chinese Medicine Publishing House: Beijing, China, 1996.
5. Xu, R.; Zhong, F.L.; Wu, D.F. Textual research on Chinese herbal medicine Qingpi. *J. Chin. Med. Mater.* **2013**, *36*, 1018–1023.
6. Huang, H.; Zeng, C.H.; Mao, S.J.; Liang, R.X. Effects of Qingpi and vinegar-made Qingpi on isolated intestinal motility. *J. Jiangxi Univ. Chin.* **2005**, *17*, 52–53.
7. Zhao, Y.S.; Huang, W.; Wang, X.Y.; Chen, H.P.; Liu, Y.P. Effects of Chenpi and Qingpi on the Motility of Isolated Rabbit Intestinal Muscle. *Liaoning J. Tradit. Chin. Med.* **2011**, *38*, 1451–1452.

8. Yang, Y.L. The effects of Zhishi and Qingpi on the motivity of smooth muscle. *J. Northwest Norm. Univ. (Nat. Sci.)* **2002**, *38*, 114–117.
9. Chen, K.; Ye, Q. Effects of processing on flavonoids in Qingpi. *J. Chin. Med. Mater.* **1996**, *19*, 185–186.
10. Yang, Y.L.; Zhen, T.Z.; Qu, S.Y.; Li, W.; Xie, D.P.; Ding, Y.H.; Wei, Y.L. Effects of Qingpi and Chenpi on the movement of longitudinal muscle strips in the small intestine of rats. *J. Lanzhou Univ. Nat. Sci.* **2001**, *37*, 94–97.
11. Zhang, Y.; Zhang, H.; Wu, D.X. Effects of traditional Chinese medicine for treating “liver” on gastrointestinal bioelectricity and blood flow. *China J. Tradit. Chin. Med. Pharm.* **1989**, *4*, 26–29.
12. Kang, S.A.; Park, H.J.; Kim, M.J.; Lee, S.Y.; Han, S.W.; Leem, K.H. Citri Reticulatae Viride Pericarpium extract induced apoptosis in SNU-C4, human colon cancer cells. *J. Ethnopharmacol.* **2005**, *97*, 231–235. [[CrossRef](#)]
13. Zeng, S.L.; Li, S.Z.; Xiao, P.T.; Cai, Y.Y.; Chu, C.; Chen, B.Z.; Li, P.; Li, J.; Liu, E.H. Citrus polymethoxyflavones attenuate metabolic syndrome by regulating gut microbiome and amino acid metabolism. *Sci. Adv.* **2020**, *6*, eaax6208. [[CrossRef](#)]
14. Gao, Z.; Wang, Z.Y.; Guo, Y.; Chu, C.; Zheng, G.D.; Liu, E.H.; Li, F. Enrichment of polymethoxyflavones from Citrus reticulata ‘Chachi’ peels and their hypolipidemic effect. *J. Chromatogr. B Anal. Technol. Biomed. Life Sci.* **2019**, *1124*, 226–232. [[CrossRef](#)]
15. Wang, Y.; Chen, Y.; Zhang, H.; Chen, J.; Cao, J.; Chen, Q.; Li, X.; Sun, C. Polymethoxyflavones from citrus inhibited gastric cancer cell proliferation through inducing apoptosis by upregulating RARbeta, both in vitro and in vivo. *Food Chem. Toxicol.* **2020**, *146*, 111811. [[CrossRef](#)]
16. Lin, Z.H.; Chan, Y.F.; Pan, M.H.; Tung, Y.C.; Su, Z.Y. Aged citrus peel (Chenpi) prevents Acetaminophen-Induced hepatotoxicity by epigenetically regulating nrf2 pathway. *Am. J. Chin. Med.* **2019**, *47*, 1833–1851. [[CrossRef](#)]
17. Funaguchi, N.; Ohno, Y.; La, B.L.; Asai, T.; Yuhgetsu, H.; Sawada, M.; Takemura, G.; Minatoguchi, S.; Fujiwara, T.; Fujiwara, H. Narirutin inhibits airway inflammation in an allergic mouse model. *Clin. Exp. Pharmacol. Physiol.* **2007**, *34*, 766–770. [[CrossRef](#)]
18. Chen, X.M.; Tait, A.R.; Kitts, D.D. Flavonoid composition of orange peel and its association with antioxidant and anti-inflammatory activities. *Food Chem.* **2017**, *218*, 15–21. [[CrossRef](#)]
19. Hagenlocher, Y.; Gommeringer, S.; Held, A.; Feilhauer, K.; Koninger, J.; Bischoff, S.C.; Lorentz, A. Nobiletin acts anti-inflammatory on murine IL-10(-/-) colitis and human intestinal fibroblasts. *Eur. J. Nutr.* **2019**, *58*, 1391–1401. [[CrossRef](#)]
20. Guvenc, M.; Cellat, M.; Gokecek, I.; Ozkan, H.; Arkali, G.; Yakan, A.; Yurdagul, O.S.; Aksakal, M. Nobiletin attenuates acetaminophen-induced hepatorenal toxicity in rats. *J. Biochem. Mol. Toxicol.* **2020**, *34*, e22427. [[CrossRef](#)]
21. Li, M.; Zhao, Y.; Qi, D.; He, J.; Wang, D. Tangeretin attenuates lipopolysaccharide-induced acute lung injury through Notch signaling pathway via suppressing Th17cell response in mice. *Microb. Pathog.* **2020**, *138*, 103826. [[CrossRef](#)]
22. Zheng, J.; Shao, Y.; Jiang, Y.; Chen, F.; Liu, S.; Yu, N.; Zhang, D.; Liu, X.; Zou, L. Tangeretin inhibits hepatocellular carcinoma proliferation and migration by promoting autophagy-related BECLIN1. *Cancer Manag. Res.* **2019**, *11*, 5231–5242. [[CrossRef](#)]
23. Ha, S.K.; Park, H.; Eom, H.; Kim, Y.; Choi, I. Narirutin fraction from citrus peels attenuates LPS-stimulated inflammatory response through inhibition of NF- κ B and MAPKs activation. *Food Chem. Toxicol.* **2012**, *50*, 3498–3504. [[CrossRef](#)]
24. Chakraborty, S.; Basu, S. Multi-functional activities of citrus flavonoid narirutin in Alzheimer’s disease therapeutics: An integrated screening approach and in vitro validation. *Int. J. Biol. Macromol.* **2017**, *103*, 733–743. [[CrossRef](#)]
25. Park, H.Y.; Ha, S.K.; Eom, H.; Choi, I. Narirutin fraction from citrus peels attenuates alcoholic liver disease in mice. *Food Chem. Toxicol.* **2013**, *55*, 637–644. [[CrossRef](#)]
26. Chen, H.; Nie, T.; Zhang, P.; Ma, J.; Shan, A. Hesperidin attenuates hepatic lipid accumulation in mice fed high-fat diet and oleic acid induced HepG2 via AMPK activation. *Life Sci.* **2022**, *296*, 120428. [[CrossRef](#)]
27. Zhang, M.; Chen, D.; Zeng, N.; Liu, Z.; Chen, X.; Xiao, H.; Xiao, L.; Liu, Z.; Dong, Y.; Zheng, J. Hesperidin Ameliorates Dexamethasone-Induced Osteoporosis by Inhibiting p53. *Front. Cell Dev. Biol.* **2022**, *10*, 820922. [[CrossRef](#)]
28. Li, X.R.; Ma, Z.J.; Mao, S.J.; Ma, Y.; Yang, J.Y.; Cheng, L.P. Content comparison of four components in Geqingpi and Sihuaqingpi. *Chin. Tradit. Pat. Med.* **2005**, *27*, 611–612.
29. Chen, F.; Liang, Y.Y.; Tong, P.Z.; Wang, L.W.; Liu, X.X.; Sun, D.M.; Li, G.W. UPLC Fingerprint of Citri Reticulatae Pericarpium Viride in Different Specifications. *Mod. Chin. Med.* **2021**, *23*, 117–122.
30. He, X.; Huang, S.; Wu, M.; Wu, M.; Zhang, Y.; Ma, Z.; Liu, L.; Cao, H. Simultaneous quantitative analysis of ten bioactive flavonoids in Citri Reticulatae Pericarpium Viride (Qing Pi) by ultrahigh-performance liquid chromatography and high-resolution mass spectrometry combined with chemometric methods. *Phytochem. Anal.* **2021**, *32*, 1152–1161. [[CrossRef](#)]
31. Li, P.L.; Liu, M.H.; Hu, J.H.; Su, W.W. Systematic chemical profiling of Citrus grandis ‘Tomentosa’ by ultra-fast liquid chromatography/diode-array detector/quadrupole time-of-flight tandem mass spectrometry. *J. Pharm. Biomed. Anal.* **2014**, *90*, 167–179. [[CrossRef](#)]
32. Cuyckens, F.; Rozenberg, R.; de Hoffmann, E.; Claeys, M. Structure characterization of flavonoid O-diglycosides by positive and negative nano-electrospray ionization ion trap mass spectrometry. *J. Mass Spectrom.* **2001**, *36*, 1203–1210. [[CrossRef](#)]
33. Abad-Garcia, B.; Garmon-Lobato, S.; Berrueta, L.A.; Gallo, B.; Vicente, F. Practical guidelines for characterization of O-diglycosyl flavonoid isomers by triple quadrupole MS and their applications for identification of some fruit juices flavonoids. *J. Mass Spectrom.* **2009**, *44*, 1017–1025. [[CrossRef](#)]
34. Zheng, Y.Y.; Zeng, X.; Peng, W.; Wu, Z.; Su, W.W. Characterisation and classification of Citri Reticulatae Pericarpium varieties based on UHPLC-Q-TOF-MS/MS combined with multivariate statistical analyses. *Phytochem. Anal.* **2019**, *30*, 278–291. [[CrossRef](#)]
35. Monika, A.O.; Joanna, M.R. Phenolic constituents of the inflorescences of *Sorbus torminalis* (L.) Crantz. *Phytochem. Lett.* **2011**, *4*, 151–157.

36. Ye, X.L. The Study on Chemical Fingerprint and Metabolic Profile of Citrus Reticulate 'Chachi'. Master Thesis, Guangdong Pharmaceutical University, Guangzhou, China, 2013.
37. Liu, M.S.; Yang, D.P.; Yang, W.L.; Cai, Y.; Wang, K.H.; Peng, M.D.; Chen, B.Z.; Zheng, G.D. Analysis of compounds in Citri Reticulatae Pericarpium Virde by UHPLC-Q-Exactive Orbitrap-MS. *Chin. J. Hosp. Pharm.* **2021**, *41*, 2395–2400.
38. Zeng, X.; Su, W.; Zheng, Y.; Liu, H.; Li, P.; Zhang, W.; Liang, Y.; Bai, Y.; Peng, W.; Yao, H. UFLC-Q-TOF-MS/MS-Based screening and identification of flavonoids and derived metabolites in human urine after oral administration of exocarpium citri grandis extract. *Molecules* **2018**, *23*, 895. [[CrossRef](#)]
39. Beatriz, A.; Sergio, G.; Luis, A.B.; Blanca, G.; Francisca, V. On line characterization of 58 phenolic compounds in Citrus fruit juices from Spanish cultivars by high-performance liquid chromatography with photodiode-array detection coupled to electrospray ionization triple quadrupole mass spectrometry. *Talanta* **2012**, *99*, 213–224.
40. Zheng, G.D.; Zhou, P.; Yang, H.; Li, Y.S.; Li, P.; Liu, E.H. Rapid resolution liquid chromatography-electrospray ionisation tandem mass spectrometry method for identification of chemical constituents in Citri Reticulatae Pericarpium. *Food Chem.* **2013**, *136*, 604–611. [[CrossRef](#)]
41. Xing, T.T.; Zhao, X.J.; Zhang, Y.D.; Li, Y.F. Fast separation and sensitive quantitation of polymethoxylated flavonoids in the peels of citrus using UPLC-Q-TOF-MS. *J. Agric. Food Chem.* **2017**, *65*, 2615–2627. [[CrossRef](#)]
42. Liu, H.; Zhao, H.; Che, J. Naringenin alleviates obesity-associated hypertension by reducing hyperlipidemia and oxidative stress. *Kidney Blood Press Res.* **2022**. [[CrossRef](#)]
43. Wang, Q.; Ou, Y.; Hu, G.; Wen, C.; Yue, S.; Chen, C.; Xu, L.; Xie, J.; Dai, H.; Xiao, H.; et al. Naringenin attenuates non-alcoholic fatty liver disease by down-regulating the NLRP3/NF-kappaB pathway in mice. *Br. J. Pharm.* **2020**, *177*, 1806–1821. [[CrossRef](#)]
44. Ammar, N.M.; Hassan, H.A.; Abdallah, H.M.I.; Afifi, S.M.; Elgamal, A.M.; Farrag, A.R.H.; El-Gendy, A.E.G.; Farag, M.A.; Elshamy, A.I. Protective Effects of Naringenin from *Citrus sinensis* (var. Valencia) Peels against CCl4-Induced Hepatic and Renal Injuries in Rats Assessed by Metabolomics, Histological and Biochemical Analyses. *Nutrients* **2022**, *14*, 841. [[CrossRef](#)]
45. Muhammad, T.; Ikram, M.; Ullah, R.; Rehman, S.U.; Kim, M.O. Hesperetin, a citrus flavonoid, attenuates LPS-Induced neuroinflammation, apoptosis and memory impairments by modulating TLR4/NF-kappaB signaling. *Nutrients* **2019**, *11*, 648. [[CrossRef](#)]
46. Ikram, M.; Muhammad, T.; Rehman, S.U.; Khan, A.; Jo, M.G.; Ali, T.; Kim, M.O. Hesperetin confers neuroprotection by regulating Nrf2/TLR4/NF-κB signaling in an aβ mouse model. *Mol. Neurobiol.* **2019**, *56*, 6293–6309. [[CrossRef](#)]
47. Wang, L.; Jing, S.; Qu, H.; Wang, K.; Jin, Y.; Ding, Y.; Yang, L.; Yu, H.; Shi, Y.; Li, Q.; et al. Orientin mediates protection against MRSA-induced pneumonia by inhibiting Sortase a. *Virulence* **2021**, *12*, 2149–2161. [[CrossRef](#)]
48. Fang, J.; Cao, Z.; Song, X.; Zhang, X.; Mai, B.; Wen, T.; Lin, J.; Chen, J.; Chi, Y.; Su, T.; et al. Rhoifolin Alleviates Inflammation of Acute Inflammation Animal Models and LPS-Induced RAW264.7 Cells via IKKbeta/NF-kappaB Signaling Pathway. *Inflammation* **2020**, *43*, 2191–2201. [[CrossRef](#)]
49. Peng, S.; Hu, C.; Liu, X.; Lei, L.; He, G.; Xiong, C.; Wu, W. Rhoifolin regulates oxidative stress and proinflammatory cytokine levels in Freund's adjuvant-induced rheumatoid arthritis via inhibition of NF-κB. *Braz. J. Med. Biol. Res.* **2020**, *53*, e9489. [[CrossRef](#)]
50. Zheng, B.; Zheng, Y.; Zhang, N.; Zhang, Y.; Zheng, B. Rhoifolin from Plumula Nelumbinis exhibits anti-cancer effects in pancreatic cancer via AKT/JNK signaling pathways. *Sci. Rep.* **2022**, *12*, 5654. [[CrossRef](#)]
51. Tsai, Y.C.; Wang, S.L.; Wu, M.Y.; Liao, C.H.; Lin, C.H.; Chen, J.J.; Fu, S.L. Pilloin, a Flavonoid Isolated from *Aquilaria sinensis*, Exhibits Anti-Inflammatory Activity in Vitro and in Vivo. *Molecules* **2018**, *23*, 3177. [[CrossRef](#)]